Title: Cellular contributions to ictal population signals

Authors: Lauren A. Lau[1], Zhuoyang Zhao[1], Stephen N. Gomperts[1], Kevin J. Staley[1*] and Kyle P. Lillis[1]

Affiliations:

[1]Massachusetts General Hospital, Department of Neurology, Boston, Massachusetts 02114, Harvard Medical School, Boston, Massachusetts 02115.

*Corresponding author. Email: Staley.kevin@mgh.harvard.edu

One Sentence Summary: The ictal signal is primarily driven by increased amplitude of signals in individual neurons, with the remainder coming from network synchrony.

Abstract: The amplitude of ictal activity is a defining feature of epileptic seizures, but the determinants of this amplitude have not been identified. Clinically, ictal amplitudes are measured electrographically (using e.g. EEG, ECoG, and depth electrodes), but these methods do not enable the assessment of individual neurons. Spontaneous seizure activity was assessed here in an awake, behaving mouse model of focal cortical injury and in organotypic hippocampal slice cultures (OHSC), an in vitro preparation from which recurrent seizures can be readily captured. We measured population activity by simultaneously recording electrographic local field potentials and imaging the activity of individual neurons with genetically encoded calcium indicators (GECI). We further linked the electrical activity and calcium signal of individual neurons, by performing simultaneous GECI-based calcium imaging and whole-cell patch-clamp recordings in OHSCs. Activity was analyzed in three epochs: interictal, seizure onset, and ictal. Population signal may increase from three potential sources: 1) increased synchrony, i.e. more co-active neurons, 2) altered active state, from bursts of action potentials and/or paroxysmal depolarizing shifts in membrane potential, and 3) altered subthreshold state, which includes all lower levels of activity. The largest contributor to the signal recorded at seizure onset was increased subthreshold activity, consistent with barrages of excitatory postsynaptic potentials. The relative contribution of synchronous activity increased during ictal periods, but the increased amplitude of intra-cellular discharges, both subthreshold and active, remained the largest driver of the ictal signal. This study provides a critical link between single neuron activity and population measures of seizure activity.

Main Text:

INTRODUCTION

The amplitude of paroxysmal ictal activity is a defining feature of epileptic seizures. Although low-amplitude seizures occur, for example in infantile spasms (*1*), this is the exception. The rule is that seizure activity is recognizable in electroencephalographic recordings in large part because of the distinguishing increase in EEG amplitude (*2, 3*). However, despite the central role of EEG in diagnosing epilepsy and localizing seizure foci for surgical planning, the determinants of this unique increase in amplitude remain unclear. Here we identify those determinants.

The EEG signal is a nonlinear summation of the activity of the neurons and glia in the underlying cortex (*4, 5*). A well-known contributor to the ictal signal is the paroxysmal depolarizing shift (PDS) in the neuronal membrane potential, which lasts hundreds of milliseconds (*6, 7*). Lower-amplitude synaptic activity also contributes to the ictal EEG, including the barrages of excitatory postsynaptic potentials that are thought to trigger the PDS and propagate seizure activity (*8, 9*). Network synchrony is another key seizure characteristic. Scalp EEG reports a spatial average of underlying cortical activity, and only activity that is synchronous across the reported cortical volume is recognizable in the scalp EEG (*10*). Epileptiform EEG has therefore been considered to represent highly synchronous activity of cortical neurons (*5, 9*). Increased synchrony can arise from recurrent activation of neurons, or the recruitment of new populations of neurons (*11*).

Electrophysiological methods have been used to record the activity of individual neurons with high temporal and moderate spatial resolution during physiological activity and, in some cases, even during seizure onset (*11, 12*). However, these methods are limited to capturing the spiking activity of neurons. Action potentials are too brief to be reflected in EEG, thus capturing the spiking activity from individual neurons does not provide the means to understand the population-level signal. To capture the relevant activities of individual neurons, we combined whole-cell recordings of the membrane potential with field potential recordings and optical imaging of calcium using the genetically encoded calcium indicator GCaMP. Small fluctuations in calcium accompany postsynaptic potentials, as calcium enters through ionotropic glutamate receptors and certain classes of voltage-gated calcium channels (*13-15*). Neuronal spiking and PDS both drive high calcium signal (*16, 17*). In addition to these cell-intrinsic signals, network synchrony can also be measured in a straightforward way with calcium imaging. Thus, recordings with high spatial resolution and sensitivity to a wide dynamic range of signals can be obtained over a large cortical volume, allowing for the precise quantification of the total number of active neurons.

Simultaneous microendoscope calcium imaging and local field potential recordings are now feasible in awake, behaving murine models of focal cortical injury (*18*) (where seizures were observed following cortical aspiration in the seizure susceptible APP/PS1 mouse (*19*)). However, spontaneous seizures while the subject is being recorded are exceptionally rare events, and only a single partial spontaneous ictal recording has been reported to date (*20*). The current report is based on the serendipitous recordings of several such spontaneous seizures *in vivo*. To extend these rare in vivo findings, we also performed multimodal recordings in a reduced, chronically epileptic preparation: the organotypic hippocampal slice culture (OHSC). Unlike the in vivo model, seizures in OHSC are frequent and straightforward to capture during an imaging session.

Additionally, cellular resolution recordings can be obtained from the entire epileptic network and contributions to ictal signal can be unambiguously ascribed to the seizure focus (*21*).

We developed novel methods to quantify the relative contribution of inter-cellular (i.e. synchronization) and intra-cellular sources to the overall ictal signal. During seizure onset the majority of the signal increase was driven by increased amplitude of the discharges of individual neurons, with the role of network synchrony becoming more prominent during the transition to frank seizure. We further show that synchronous activity during seizure is dominated by reactivation of neurons, rather than the recruitment of new populations of neurons into the seizure. This work provides a framework for the careful quantification of the underlying sources to populations signals that can be applied in multiple models and both physiological and pathological brain states.

RESULTS

Genetically encoded calcium indicators (GECIs) to simultaneously record single cell and population seizure activity

To demonstrate the relationship between the calcium signal and epileptiform electrical activity at the single neuron level, we performed simultaneous whole-cell patch clamp recordings and two-photon soma-GCaMP8m calcium imaging in the OHSC model (Figure 1), which generates spontaneous recurrent seizure-like events (henceforth referred to as seizures), beginning approximately 1-week post-slicing injury (*22*). To quantify when neurons are active (based on the calcium signal alone), a detection threshold was employed to separate subthreshold and active states. The detection threshold was calculated on a cell-by-cell basis, from a period of non-epileptiform activity (see Methods for details). During inter-ictal periods, the subthreshold state is characterized by a relatively stable, low amplitude calcium signal. The calcium amplitude of individual neurons was lowest during this period (Figure 1, n = 3 neurons from 3 OHSCs) and was characterized by a low frequency (<1 Hz) of excitatory postsynaptic potentials (EPSPs). In the inter-ictal period, 82% of single action potential (AP) events produced a detectable rise in the calcium signal into the active state in the following 300 ms (n =1 cell, with AP firing between seizures). 100% of 2+ action potential events, with an inter-spike interval less than 150 ms, produced an active state calcium response. This is in line with previous reports on the sensitivity of GGaMP to detect neuronal spiking (*17, 23*).

During seizure onset, we observed that a barrage of EPSPs (frequency >4 Hz) is capable of driving an increase in the amplitude of the calcium signal (Figure 1, n = 3 neurons), which still remained subthreshold (i.e., below our defined active state detection threshold). Isolated action potentials (inter-spike interval > 150 ms) were frequently observed during seizure onset and resulted in higher amplitude calcium signal. In comparison to APs generated during inter-ictal activity, 100% of APs fired during seizure were correlated with an active state calcium response. Clusters of action potentials (defined as 10+ APs with inter-spike interval <150 ms) were consistently seen during spontaneous seizures and drove the calcium amplitude even higher. Paroxysmal depolarizing shifts were also observed during seizure activity and were associated with the highest amplitude calcium signal (Figure 1).

The network calcium signal can easily be obtained by averaging the calcium signal of all neurons in the field of view. **Seizures** were defined from the population-level calcium signal as periods of high amplitude calcium events lasting >10 seconds that coincided with increased amplitude in at least 1 channel of the LFP (Figure 2C-F). Rarely, in vivo seizures were observed where the increased amplitude in calcium was apparent tens of seconds earlier than the increased amplitude in the LFP (possibly due to the imaged cells falling outside of the electrical field detected by the LFP electrode). These seizures were analyzed as a separate class of seizures (Supplemental Figure 1). **Seizure onset** was defined as the period of relatively lower amplitude activity when the population calcium could first be distinguished from inter-ictal activity until the transition to **frank seizure**- marked by a local maximum in the population calcium slope (Figure 2E and F). Frank seizure is also referred to as **ictal** activity.

We recorded neuronal-resolution calcium activity both in vivo and in vitro. The in vivo recordings describe spontaneous seizures in awake, behaving animals. Recordings utilized a miniaturized fluorescence microscope and gradient refractive index (GRIN) lens in APP1/PS1 mice that had a cortical injury due to cortical aspiration/GRIN lens implantation (Figure 2A). APP/PS1 mutations are associated with early-onset Alzheimer's (*24*), and increased seizure susceptibility (*19*). In our experience, these mice will occasionally develop spontaneous seizures after a cortical aspiration injury. In this study, we recorded only non-convulsive seizures due to limitations in imaging during convulsive seizures. Imaging of neuronal calcium activity was done with the genetically encoded calcium indicator (GECI) syn-GCaMP6f and was paired with recording of the local field potential (LFP) and unit activity from 7 stereotrodes sampling the nearby cortical and hippocampal areas (as detailed in (*25, 26*)).

Capturing *spontaneous*, non-convulsive seizures in vivo is rare. Furthermore, the limited field of view in vivo does not allow for definitive identification of the seizure onset zone. We therefore also performed syn-GCaMP7f based calcium imaging in vitro, in the OHSC model (Figure 2B). Due to the reduced size of the OHSC, the entire network can be sampled, guaranteeing that we capture activity from the seizure focus (versus strictly propagated activity, as is likely to be the case in vivo). In both models, the somatic calcium signal from hundreds of individual neurons was extracted (Figure 2C-D), and calcium signals were corrected for motion, neuropil contamination and normalized as $\Delta f/f$ (see Methods (*21*)).

We found a high correlation between the optical recordings of neuronal calcium activity and the LFP electrophysiological recordings of population activity. To compare the two modalities in vivo, we transformed the LFP by filtering for multiunit activity (MUA), rectifying, and down-sampling the data to 20 Hz (to match the imaging rate). After convolving with the decay kinetics of GCaMP6f (*17*), we found a correlation of 0.7-0.84 between the mean population calcium activity and the MUA activity, with the highest correlation occurring in the LFP channel closest to the site of imaging (Figure 2G and H). Similarly, to compare the two modalities in vitro, we transformed the LFP data by rectifying, down-sampling to 35 Hz (to match the imaging rate) and convolving with GCaMP7f decay kinetics (*27*) and found a correlation of 0.96 between the calcium signal and electrophysiology (Figure 2I and J). The comparatively higher correlation between population calcium and the LFP observed in vitro is likely due to the complete sampling of all neurons in the network (whereas sampling of all neurons in vivo is not possible, and neurons outside of the imaging field of view are likely to be contributing to the electrical activity).

Calcium imaging to dissect population activity

Calcium imaging can thus be used to make inferences about several types of neuronal activity. Single cell calcium signals can be averaged in a straightforward manner to calculate the network calcium signal (Figure 3A-B). The fraction of active neurons was used to assess network **synchrony** (Figure 3C-E). Synchrony could be further separated into **recruitment** (i.e. new activation) and reactivation. Recruitment was based on each seizure event (from seizure onset to the end of the ictal period) such that, the first time a neuron was active in a seizure epoch was considered the recruitment point. Each neuron could only be recruited once per seizure, and activity prior to seizure onset did not inform recruitment. **Reactivation** refers to any time a neuron is in the active state after the initial recruitment point and includes both continued activity of a neuron after initial recruitment or renewed activation after a period of inactivity. In addition to changes in network synchrony, the amplitudes of the calcium signal in both the subthreshold and active states vary, consistent with differing modes of activity (Figure 3F). Together the changes in intra-cellular calcium amplitude, recruitment, and reactivation underly the population level ictal signal (Figure 3).

Network synchrony during seizure

To quantify synchronous activity, we used the instantaneous fraction of active neurons (where fraction synchronously active (S) = # active neurons / total # of GCaMP-positive neurons, in each time frame of either 28 ms (OHSC) or 50 ms (in vivo)). During interictal activity, the mean fraction active was very low (0.2% ± 0.003, n = 82 recordings OHSC; 0.49% ± 0.08, n = 3 recordings in vivo). This interictal sample ranged from 11-56 seconds, depending on how much pre-seizure activity was captured. Across the same time period, 47.0% ± 0.6 (OHSC) and 7.2% ± 2.2 (in vivo) of neurons are active (above detection threshold) at least once, revealing low levels of asynchronous activity inter-ictally. The time-averaged fraction of synchronously active cells increased during seizure onset (Figure 3E and 4A,C and E, mean percentage active 6.7% ± 0.6, n = 82 seizures in OHSC; Figure 4B,D and F, mean percentage active 8.2% ± 2.2, n = 5 seizures in vivo). Increased synchrony was even more pronounced during ictal activity (mean percentage active: 47.1% ± 1.9, over the first 10 seconds of frank seizure activity in OHSC; 20.0% ± 4.2 over entire ictal period in vivo). The percent active at each time point is calculated independently, and different neurons contribute to network synchrony at each time point.

New recruitment accounted for 32.2% ± 2.4 and 0.4% ± 0.2 of the total active fractions during onset and frank seizure in OHSC, (Figure 4E). In vivo, new recruitment constitutes 2.7% ± 1.8 and 0.4% ± 0.2 of the total active fractions during onset and frank seizure activity, with the vast majority of the active signal coming from reactivation of neurons that had already been recruited into the seizure (Figure 4F). The rate of new recruitment in OHSC was 32.5% ± 2.3 of total network recruited per second during onset and 2.0% ± 0.2 during frank seizure (Fig 4G and I); recruitment in vivo was much slower and occurred at a rate of 1.3% ± 0.01 (onset) and 1.0% ± 0.01 (ictal) (Figure 4H and K). In total, 78.6% ± 2.0 of neurons were recruited during seizure onset in OHSC, with the remaining 21.0% ± 2.0 of the neuronal population recruited during ictal activity, for a total cumulative recruitment of 99.6% ± 0.1 (Figure 4J). This reveals that the transition to frank seizure is largely due to synchronous activation of previously recruited neuronal populations in the organotypic hippocampal slice culture. In vivo, 23.7% ± 6.3 of neurons were recruited during seizure onset and 39.5% ± 6.0 during the ictal period, for a total cumulative recruitment of 63.2% ± 11.5 (Figure 4L). In vivo, while synchronous activity is predominately driven by reactivation, a significant number of neurons are being newly recruited

during seizure progression. These differences in recruitment are likely due to differences in the models (where there are far more neurons available to recruit in vivo versus in vitro). But the differences may also reflect both slower and less total recruitment occurring outside of the seizure focus. In vitro recordings were always in the seizure focus, but in vivo recordings may be either in the focus or in the propagation area of a particular seizure.

Dynamics of the intra-cellular calcium amplitude

Prior to seizure onset, neurons display a relatively stable subthreshold calcium amplitude (Figure 5A). To quantify the change in intra-cellular calcium amplitude during seizure onsets and ictal activity, we first identified a baseline period of non-ictal activity (without seizure or epileptiform activity). From this period, we calculated the mean baseline subthreshold (ST) calcium amplitude ($STCa^{+2}_{t=0}$) for each neuron by averaging all subthreshold values during the baseline window. We then normalized the subthreshold calcium amplitude ($\overline{STCa^{+2}}$) by dividing by the baseline $STCa^{+2}_{t=0}$ (Figure 5C). The normalized $STCa^{+2}$ provided a measure of the fold increase in subthreshold calcium amplitude during seizure onset and frank seizure. On average, the mean fold increase of the subthreshold calcium amplitude during seizure onset was 1.36 ± 0.02 (n = 82 seizures) in OHSC, and 1.68 ± 0.21 (n = 5 seizures) in vivo (Figure 5E and F). During frank seizure, the average fold increase in $STCa^{+2}$ amplitude was 2.03 ± 0.02 in OHSC, and 1.80 ± 0.42 in vivo (Figure 5E-F). While, by definition, neurons are in the subthreshold state at all points when they are included in the $STCa^{+2}$ population, on average the subthreshold calcium amplitude is significantly increased during seizure onset ($p < 0.001$ OHSC; $p = 0.01$ in vivo, paired t-test) and frank seizure ($p < 0.001$ OHSC; $p = 0.01$ in vivo). To address the possibility of neuropil contamination driving this increase, we hand-drew the regions of interest in a subset of neurons in OHSC (Supplemental Figure 2A). In this case, nearly complete neuropil subtraction can be performed (see Methods) and the increased subthreshold amplitude persists (Supplemental Figure 2B; $p = 0.003$ and $p < 0.001$, for onset and ictal period respectively). We also performed cellular resolution two-photon imaging of calcium with soma-targeted GCaMP8m during seizure in OHSC. These conditions greatly reduce the contribution of neuropil contamination, and the significant increase in subthreshold calcium amplitude is still observed (Supplemental Figure 2C; $p < 0.001$ for onset and ictal amplitude change). Due to the sustained nature of the increase, sparse firing that remains below the detection threshold is unlikely to account for the increase. Rather we predict that the subthreshold increase in calcium is due to intra-cellular calcium influx, perhaps from postsynaptic potentials activating low voltage-activated calcium channels. We further confirmed that subthreshold calcium amplitude can change independently from changes in the mean Δf/f signal. During sharp wave ripples recorded in vivo from non-seizing animals, the mean calcium signal decreases (*25*) compared to REM sleep, however in this same period subthreshold calcium amplitude increased significantly (n = 134 neurons, $p < 0.001$, paired t-test, extended analysis of dataset published in Zhou et al.(*25*, *28*)).

During seizure, the calcium amplitude of individual neurons also increased for the active state (Figure 5B and D). The baseline active calcium amplitude ($ActCa^{+2}_{t=0}$) was calculated for each neuron by averaging all active state values during the baseline time period. On average, the fold increase of the active calcium amplitude during seizure onset was 1.08 ± 0.006 in OHSC (n = 82 seizures; $p < 0.001$ paired t-test), and 1.20 ± 0.13 in vivo (n = 5 seizures; $p = 0.09$) (Figure 5G-H). During frank seizure, the average fold increase in active calcium amplitude was 1.37 ± 0.02 in OHSC ($p < 0.001$), and 1.40 ± 0.17 in vivo ($p = 0.04$) (Figure 5G-H). The observed increase in

calcium amplitude is present even when accounting for the slower decay kinetics of GCaMP (Supplemental Figure 3A-C). This reveals that neurons do not enter a static "active" state, but rather, that intra-cellular perturbations allow for higher levels of calcium signal to occur during seizure, perhaps through high frequency action potential firing (*29*), action potential broadening (*30*), and/or PDS (*31*).

How synchrony and calcium amplitude changes contribute to total seizure activity

With synchrony and intra-cellular calcium amplitude precisely quantified on the individual neuron scale, the relative contribution of each source to population means can be calculated (Figure 6). The fraction of the increased population signal that comes from synchronous activity, as either recruitment or reactivation, is calculated compared to 0% activation. The fraction from active state and subthreshold amplitude changes is calculated compared to the same level of activity, with active state and subthreshold amplitudes equal to amplitudes calculated during inter-ictal, non-epileptiform activity (See Methods for details). The total contribution from active state neurons is represented by the summation of the contributions from network synchrony and increased $ActCa^{+2}$ amplitude. On average in OHSC, the contributions to the increased population signal during seizure onset are 9.0% ± 0.8 recruitment, 17.3% ± 0.1 re-activation, 4.3% ± 0.5 increase in $ActCa^{+2}$ amplitude, and 69.4% ± 1.5 increase in $STCa^{+2}$ amplitude (n = 82 seizures; Figure 6C). In vivo, the increase in the population mean during seizure onset is 0.2% ± 0.02 recruitment, 19.7% ± 1.5 re-activation, 21.4% ± 2.0 increase in $ActCa^{+2}$ amplitude, and 58.9% ± 3.3 increase in $STCa^{+2}$ amplitude (n = 5 seizures; Figure 6F). This substantiates a new finding that the majority of the signal increase during seizure onset is due to changes in the amplitude of intra-cellular calcium in neurons while they are in the subthreshold calcium state. In other words, there are widespread, low-level calcium increases during seizure onset.

During frank seizure in OHSC, the population signal arises from: 0.9% ± 0.1 recruitment, 46.5% ± 0.7 re-activation, 25.5% ± 1.2 $ActCa^{+2}$ amplitude, and 27.1% ± 1.6 $STCa^{+2}$ amplitude (Figure 6C). In vivo, the ictal population signal is 0.03% ± 0.01 recruitment, 29.3% ± 1.8 re-activation, 34.6% ± 3.3 increased $ActCa^{+2}$ amplitude, and 36.1% ± 4.8 increased $STCa^{+2}$ amplitude (Figure 6F). While subthreshold amplitude changes are still a significant factor during frank seizure, the relative contribution from active state neurons increases during ictal activity (Figure 7B-C), with high levels of sustained activity in previously recruited cells. The contribution of network synchrony is particularly pronounced in the OHSC, which may suggest that synchrony is highest in the seizure focus (and relatively lower in regions of seizure propagation). Finally, to control for the limitations of single-photon imaging, we spatially down-sampled a subset of OHSC data by averaging the signal from closely apposed neurons. The main findings are unchanged (Supplemental Figure 4), suggesting that our results are likely robust to potential limitations in resolving single neurons in vivo.

DISCUSSION

The quantifiable clinical hallmark of an epileptic seizure is manifest as an increase in the amplitude of EEG. Many prior studies have evaluated the intracellular correlates of ictal activity in vivo (*7, 32*) and in vitro (*33, 34*), but there remains a gap in understanding how intracellular activity of individual neurons contributes to population-level extracellular signals. Using simultaneously recorded somatic calcium transients together with cellular and local field potentials, we found that cell intrinsic changes (i.e. the amplitude increases in individual

neurons) were the largest contributor to the increased population signal during seizure onset. The high spatial resolution of calcium imaging also allowed us to resolve neuronal recruitment dynamics, substantiating the new finding that recruitment is a minor contributor to total network synchrony during seizure.

The study of seizure onset is complicated by the fact that spontaneous seizures in an intact animal are highly unlikely to originate at the site of imaging. Without comprehensive recordings, it is impossible to determine whether the activity imaged is in fact the seizure focus or propagation of a seizure that initiated elsewhere. In vivo recordings may therefore primarily capture seizure propagation. We were surprised to find that the change in subthreshold calcium activity was the single largest contributor to population activity during seizure onset in vivo. One way in which elevated subthreshold calcium amplitude could be maintained is through the combination of increased excitatory and inhibitory drive (allowing EPSP-mediated calcium influx that does not induce neuronal firing)(*35*). The increased amplitude of subthreshold calcium remained the single largest contributor during frank seizure, but the relative contribution of subthreshold calcium decreased as ictal activity progressed, consistent with the gradual collapse of surround inhibition associated with seizure propagation (*36, 37*). The combined contribution of an increased number of active state neurons and the increased amplitude of activity in those cells revealed that the majority of the ictal signal is generated by active state neurons.

Conversely, the organotypic slice culture represents a "focus only" model of seizure. In this preparation, the change in subthreshold calcium activity was the largest determinant of the amplitude of population activity during seizure onset. However, during frank seizure activity, the synchronous reactivation of previously recruited neurons was the largest single contributor to population activity. This supports the idea that in the focus, inhibition has failed during ictal activity (*9, 38*). The failure of inhibition was a requisite for the onset of seizure activity in our prior modeling studies of seizures in this preparation (*39*).

This study takes advantage of unique properties of calcium imaging to address questions that microelectrodes (MEA) cannot. Approximately 97% of a pyramidal neurons surface area is dendrite (*40, 41*), supporting the idea that the extracellular field recording largely comes from postsynaptic potentials (PSPs) (*42*). Since PSPs are inherently slower than action potentials, and arrive asynchronously at different locations, the extracellular electric field they generate is temporally broad, thus summating more readily than the brief extracellular voltage transients associated with action potentials. Calcium imaging is an imperfect proxy for neuronal electrical activity but is well-suited for capturing the effects of the PSP (Figure 1 and 2). Intracellular calcium transients comprise a lowpass filtered version of neuronal spiking (similar to field potential). Even if it were technically feasible to simultaneously record the membrane voltage of a large number of neurons, there is no way to sum the 3-dimensional array of transmembrane voltages to reach the field potential. Thus, calcium imaging provides the only currently feasible means by which to sum the activity of individual members of a seizing neural population.

Recent studies have begun to use new spike sorting techniques to investigate the activity of individual neurons during seizures recorded with MEAs in human epilepsy (*11, 43*). Modeling studies of unitary LFP (the population response generated by a single neuron spiking) have also attempted to bridge the gap between individual neuronal spiking activity and population activity measures (*44-46*). Both of these approaches begin from the identified spiking of a single cell. Our findings suggest that this spiking-centric approach may miss key features of the ictal signal.

The widespread increase in subthreshold calcium suggests that during seizure onset a large population of neurons is sitting closer to action potential firing threshold. From this network state of high subthreshold activity, it may be possible to trigger synchronized, ictal activity in a variety of ways. This is in line with our previous finding that seizures do not initiate in repeatable neuronal sequences (*21*) and suggests that many neurons would be able to drive ictal responses once the network has transitioned into a state of high subthreshold calcium. When interpreting MEA spiking data during seizure activity, it will thus be important to consider that the altered *response* to the spiking may be a critical factor in delineating the transition to seizure.

Future studies will be needed to assess the mechanisms responsible for the changes to network synchrony, and the active and subthreshold calcium states. Many studies have investigated pathological synchrony during seizure, with a myriad of potential mechanisms being identified (*47-49*). Despite these efforts, no consensus has been reached on how epileptic networks synchronize, illustrating the complexity of this process. Understanding the observed intra-cellular amplitude changes may offer new insights into seizure mechanism. The relative fraction of active state calcium which comes from PDS may be parsed with pharmacological or genetic methods to inhibit L-type voltage-gated calcium channels (VGCC) which are necessary for PDS generation (*50, 51*). Our results suggest that targeting the PDS may primarily inhibit seizure propagation rather than initiation, as the contribution of altered active state amplitude primarily occurs after the seizure onset period during sustained ictal activity. Of particular interest, will be understanding the alterations in the subthreshold calcium state that occur during seizure onset. Possible mediators of the prolonged, heightened subthreshold state include interneuron activity at seizure onset (which could prevent firing despite increased excitatory post-synaptic potentials), cell intrinsic alterations to low-voltage activated channels (such as the T-type VGCC (*52*)), or changes in extracellular potassium. Understanding these complex interactions will provide new insights into seizure initiation and potentially suggest new targets for treating seizures.

MATERIALS AND METHODS

Study design

All animal protocols were approved by the Massachusetts General Hospital Subcommittee on Research and Animal Care and were conducted in accordance with the United States Public Health Service's Policy on Humane Care and Use of Laboratory Animals. Animals were housed in standard husbandry conditions. As this is a study of ictal signals, and no treatments or modifications were performed, randomization and blinding are not applicable. For the same reason, there was no control group. Rather, single cell seizure dynamics were compared to periods without epileptiform activity in the same preparation. 8 in vivo seizures were captured from one APP/PS1 mouse (male, aged 5-months) with non-convulsive seizures. 5 seizures were analyzed as Type I (Figures 2 and 4-6) and 3 as Type II (Figure S1). Capturing neuronal resolution imaging data of spontaneous seizures in vivo is extremely rare. Many in vivo calcium imaging studies have relied on acute chemo-convulsant provoked seizures in non-epileptic brains (*53-56*). To date, only a single, partial spontaneous seizure has been reported with in vivo calcium imaging (and was of insufficient resolution for single cell analysis) (*20*). In comparison, spontaneous seizure-like events (referred to here as seizures) that occur in OHSCs are frequent and highly amenable to imaging. As described previously (*21*), our in vitro imaging paradigm was designed to capture approximately 1 seizure per day from each OHSC. Imaging began

immediately after slice preparation and continued for 3 weeks. 82 seizures were captured from 10 OHSC, from 4 animals. No recorded seizures were excluded. Based on previous work which shows that seizure onset type evolves over time and that single cell sequences are stochastic during seizure recruitment (*21*), we treated each seizure as an independent event.

In vivo virus injection

Virus injection was performed as previously described (*25, 26*). The adult APP/PS1 mouse was anesthetized and head-fixed on a stereotaxic frame. A small hole overlying hippocampal CA1 at anterior-posterior (AP) -2.10 mm and medial-lateral (ML) 1.65 mm was drilled to expose the brain surface, and 1 µl of AAV1-hSyn-GCaMP6f virus solution (with a titer of ~ 1 x10^{13}/ml) was injected (dorsal-ventral (DV) -1.40 mm). After surgical closure, the animal was returned to the housing facility and was allowed to recover for 2 weeks.

Endoscope and GRIN lens implantation surgery

Surgery was performed as previously described (*25, 26*). The animal was anesthetized under isoflurane, head-fixed on a stereotaxic frame and the underlying soft tissue was cleared to expose the skull. The pial surface was exposed at two sites, one for implantation of a lens for calcium imaging (AP -2.10 mm, ML 1.50 mm), the other for insertion of a closely apposed electrophysiology probe (AP -2.80 mm, ML 2.60 mm). To prepare for lens implantation, the cortex above dorsal hippocampal CA1 was carefully aspirated with a vacuum needle. A gradient-index (GRIN) lens 4mm in length and 1mm in diameter (Inscopix) was implanted vertically just above CA1 (DV -1.2 mm from brain surface). A custom-made adjustable electrophysiology probe consisting of 7 stereotrodes was implanted (AP −2.8 mm, ML 2.6 mm from Bregma, −36 degrees relative to the AP axis, −39 degrees relative to the inter-aural axis; DV −1.7 mm from brain surface). A cerebellar screw was placed for use as ground. After closure, the animal was returned to the housing facility and allowed to recover. Three weeks later a microscope baseplate (Inscopix) was attached to the skull above the implanted GRIN lens.

In vivo calcium imaging and electrophysiology recordings

For data acquisition, the miniscope (Inscopix) was mounted onto the baseplate, and a headstage pre-amplifier (Neuralynx) was connected to the electrophysiology probe. After a 30-minute habituation period, simultaneous calcium imaging (20 Hz) and electrophysiology recordings (local field potential recordings, 2 kHz sampling; multiunit recordings 32 kHz; filtered at 0.5–900 Hz) from each intracranial electrode were acquired, as previously described (*25, 26*). Three 10-minute-long imaging sessions (with 5-minute off periods between to prevent photobleaching) were acquired with the animal in a state of quiet wakefulness. The electrophysiology signal was acquired continuously throughout the duration of the experiment.

Organotypic Hippocampal Slice Culture (OHSC) preparation

Newborn DLX-cre mouse pups (Post-natal day (P) 1-2) received intracerebroventicular (ICV) injections of AAV-hSyn-GCaMP7f. Organotypic slice cultures were prepared from P6-P8 DLX-cre mice of either sex using the membrane insert technique (*57*), as described previously (*21*). Briefly, isolated hippocampi were cut into 400 µm slices on a McIlwain tissue chopper (Mickle Laboratory Engineering) and transferred to membrane inserts (Millipore) in six-well plates. Cultures were incubated in a custom-designed imaging system at 5% CO2, 36°C in 1 mL of Neurobasal-A growth medium supplemented with 2% B27, 500 µM GlutaMAX, and 0.03 mg/ml

gentamycin (all from Invitrogen). Slices were maintained in the custom imaging system (see below).

For whole cell patch clamp experiments (Figure 1), OHSCs were prepared with the rocking coverslip method, as previously described (*58*). As above, OHSCs were prepared from P6-P8 DLX-cre mice of either sex. Slices were placed on poly-L-lysine coated glass cover slips (Electron Microscopy Sciences) in a 6-well tissue culture plate, with AAV9-soma-GCaMP8m (1 μl per mL) included in the cell culture media. Slice cultures were maintained at 37°C, in 5% CO_2 on a rocking platform. Cell culture media was changed twice a week (without further inclusion of AAV9-soma-GCaMP8m).

OHSC chronic calcium imaging and local field potential recording

On the day of slice culture preparation, the 6-well plate containing membrane slices was transferred to the custom imaging system, an inverted microscope constructed inside of a CO_2 incubator, as described previously (*21, 39*). Slices were imaged every 6 hours to obtain an 85-second time series of green fluorescence at 35 Hz to record the spatiotemporal dynamics of calcium activity.

In some experiments, imaging was paired with electrical recordings of the extracellular field potential (*21*). Slice cultures were grown directly on top of the tungsten recording electrode. Data was collected at 1 KHz using a DC amplifier (Warner Instruments) with a 0.1 KHz filter.

OHSC acute two-photon calcium imaging and whole cell recordings

In a separate set of experiments, simultaneous two-photon calcium imaging and whole cell current clamp recordings were performed. For imaging/patching experiments, individual coverslips with OHSCs were transferred to the submersion chamber of a two-photon microscope between DIV 10-16. OHSCs were allowed to recover for approximately 15 minutes being perfused in cell culture media (at 1 ml/min), bubbled with 95%O_2/5% CO_2 at 33°C. Following recovery in cell culture media, perfusion was switched to aCSF (at 1ml/min, bubbled with 95%O_2/5% CO_2 at 33°C), containing (in mM) 124 NaCl, 1.25 NaH2PO4, 2.5 KCl, 26 NaHCO3, 2 CaCl2, 2 MgSO4, and 20 d-glucose.

Electrodes were pulled from borosilicate glass capillaries using a micropipette puller (Sutter Instruments) with resistance of 5–7 MΩ, filled with internal solution containing the following (in mm): 135 K+-gluconate, 5 NaCl, 2 $MgCl_2$, 10 HEPES, 0.4 Na_3GTP, 4 Na_2ATP, with osmolarity 290 mOSm, pH 7.25-7.35, adjusted with KOH. To aid in visualizing the pipette under fluorescence microscopy, 0.2% of 1mg/mL of Alexa Fluor 594 biocytin was added to the internal solution. Patching was done under 920 nm excitation, with a green 525/50 emission filter (Thor labs) to locate GCaMP-positive neurons. Resting membrane potential (RMP) was measured after whole-cell configuration was reached. Membrane potential was corrected for liquid junction potential of -14.3 mV. RMP of analyzed neurons was between -73 and -76 mV. All neurons that were recorded during spontaneous seizure activity were included (n = 3 neurons, from 3 OHSCs).

Current clamp recordings were acquired with a Multiclamp amplifier (Multiclamp 700B, Molecular Devices) with Clampex10 software (Molecular Devices). Signals were sampled at 10 KHz and filtered at 2 KHz. Recordings were made in gap-free mode to capture spontaneous action potentials and postsynaptic potentials. Simultaneous 30 Hz, two-photon calcium imaging was performed, with a 16x, 0.8N.A. water-immersion objective (Nikon), on a custom-built two-

photon microscope (see https://doi.org/10.1101/2023.02.14.528533), equipped with a Mai Tai 80MHz Ti:sapphire laser (Spectra-Physics), and a resonant-galvo-galvo scanhead (Vidrio RMR). GCaMP calcium signal was excited at 920 nm, with a bandpass emission filter at 525/50 (Chroma). Image acquisition was performed by ScanImage software (Vidrio Technologies) (*59*). Both modalities were synchronized by triggering the ScanImage acquisition with Clampex. Analysis of current clamp recordings was done with Clampex11 software and Mini Analysis Software.

Pre-processing of calcium signal

In vivo: Neuronal regions of interest (ROI) were identified with the Fiji plugin TrackMate (*60*), using a Laplacian of Gaussian filter to identify GCaMP-positive neuronal cell bodies. TrackMate was used to follow the position of the same ROI over time and correct for motion artifact. The mean pixel intensity was extracted from the somatic ROI and a surrounding anulus ROI of neuropil. The calcium traces were normalized as Δf/f, and corrected for neuropil contamination as:

$$\frac{\Delta f}{f} corrected = \frac{\Delta f}{f} soma - \left(0.95 * \frac{\Delta f}{f} neuropil\right)$$

The weighting factor 0.95 was determined empirically to maximize the subtraction while avoiding over-correction.

OHSC: GCaMP-positive cells were identified from a standard deviation projection (STD) of the high-resolution calcium recordings, which highlights pixels with dynamic signal. The Fiji plugin TrackMate (*60*) was used to automatically select ROIs. Somatic signal was corrected for neuropil contamination as:

$$F_{corrected} = F_{soma} - \left(0.8 * F_{neuropil}\right)$$

As above, the weighing factor 0.8 was determined empirically. F corrected was normalized as Δf/f, as described previously (*21*).

In a subset of neurons, the somatic and neuropil ROIs were hand drawn (Supplemental Figure 2A) to allow for high fidelity neuropil contamination correction:

$$F_{corrected} = F_{soma} - F_{neuropil}$$

In this case nearly complete neuropil subtraction can be performed, with potential contamination coming only from neuropil directly above/below the soma.

For processing of the calcium signal obtained during acute two-photon imaging and whole cell patch clamp, the somatic and surrounding neuropil ROIs were hand-drawn to isolate the calcium signal from the patched neuron. In this case, a weighing factor of 0.5 was determined to best remove neuropil contamination.

To account for the slower decay kinetics of GCaMP, in a subset of data, a deconvolution was performed with the subtraction of an exponential decay based on the kinetics of GCaMP7f (*27*) (Supplemental Figure 3C).

Separation of subthreshold and active calcium states

The calcium signal of neurons can exist in two states: subthreshold and active. We developed an automated method for separating these 2 states, by defining a detection threshold value calculated from a period of baseline inter-ictal activity. The baseline period was chosen to exclude high amplitude transients (characterized by a rapid increase in calcium amplitude). The normal variance in low amplitude calcium was then calculated to define a detection threshold which could reliable separate subthreshold and active amplitude activity.

In vivo: We identified a window of baseline activity (i.e. without seizure or epileptiform activity) on a cell-by-cell basis using the absolute value of calcium traces high-pass filtered at 0.2 Hz to isolate periods without high-amplitude calcium transients. Active state detection threshold was calculated as median + 2.5 standard deviations from the entire baseline period for each neuron. This strategy was selected by optimizing the detection of high-amplitude calcium transients (while minimizing false positives) in a sub-population of randomly selected cells. The detection thresholding process was then applied to the entire neuronal population in an automated fashion.

OHSC: A baseline window (without seizure or epileptiform activity) of approximately 3 seconds was identified in each seizure recording from the mean Δf/f trace. OHSC have inter-ictal periods of relative quiescence in all neurons, thus the same baseline window was used to calculate threshold in all neurons. Threshold was set as mean + 3 standard deviations on a cell-by-cell basis. The same detection thresholding method was used for data collected from the chronic 1-photon imaging and acute 2-photon imaging.

All analyses were performed in ImageJ (Fiji) and Matlab.

Quantification of calcium sources

The mean population calcium signal (mean Δf/f) can be calculated from 3 variables (Figure 7): the fraction of synchronously active neurons ($S = \frac{\#\left(ActCa^{+2}\right)}{total\#(neurons)}$), the mean active state calcium amplitude ($ActCa^{+2}$), and the mean subthreshold calcium amplitude ($STCa^{+2}$) as:

$$\frac{\Delta f}{f} = \left(ActCa^{+2} * S\right) + \left(STCa^{+2} * (1 - S)\right)$$

The first term represents the total contribution from active state neurons and the second from subthreshold neurons. The relative contribution of active state and subthreshold neurons can be found by diving by the total Δf/f signal (Figure 7).

We can also calculate the fractional increase from four sources during seizure. In this case, seizure (either seizure onset or frank seizure) is being compared to a reference period of physiological activity. In vivo, this was a period of quiet wakefulness without any epileptiform activity. In vitro, this was a period of inter-ictal activity. The reference period is defined here as t = 0. The exact duration of t = 0 varied depending on how much physiological activity was captured in the same recording as a seizure but was generally tens of seconds. The mean amplitude of $ActCa^{+2}$ and $STCa^{+2}$ was calculated from this period, as $ActCa^{+2}_{t=0}$ and $STCa^{+2}_{t=0}$. The contribution to the population Δf/f signal from network synchrony can then be calculated as:

$$\text{Synchrony: } \left(ActCa^{+2}{}_{t=0} * S\right) + \left(STCa^{+2}{}_{t=0} * (1 - S)\right) - STCa^{+2}{}_{t=0}$$

In other words, this is the contribution from an increasing number of active cells if the $ActCa^{+2}$ and $STCa^{+2}$ amplitude was unchanged from baseline. Network synchrony includes both recruitment and re-activation. The fraction of synchronous activity from each source can be isolated as:

Recruitment: $$\frac{ActCa^{+2}t=0 * \frac{\#\left(ActCa^{+2}recruited\right)}{total\#(neurons)}}{\left(ActCa^{+2}t=0 * S\right)}$$

Reactivation: $$\frac{ActCa^{+2}t=0 * \frac{\#\left(ActCa^{+2}reactivated\right)}{total\#(neurons)}}{\left(ActCa^{+2}t=0 * S\right)}$$

The fraction of the population signal which comes from $ActCa^{+2}$ and $STCa^{+2}$ amplitude changes can be calculated as:

Active calcium amplitude: $\left(ActCa^{+2} * S\right) - \left(ActCa^{+2}{}_{t=0} * S\right)$

Subthreshold calcium amplitude: $\left(STCa^{+2} * (1-S)\right) - \left(STCa^{+2}{}_{t=0} * (1-S)\right)$

In other words, the fractional increase is calculated as the difference in the total contribution from all neurons in the active state (or subthreshold state) and the contribution from the same number of neurons if the amplitude was the same as in the t=0 reference period.

Statistical Analysis

All data are reported as mean ± SEM. Tests of correlation were performed and reported as the Pearson correlation coefficient (r). Paired student *t*-tests were performed to test for statistical significance, as noted in text. In all cases, single neuron data was being compared to data from a reference period in the same cell. Statistical analyses were performed with Microsoft Excel or Matlab (MathWorks).

List of Supplementary Materials

Fig. S1 to S4

References and Notes

1. F. Panzica, S. Franceschetti, S. Binelli, L. Canafoglia, T. Granata, G. Avanzini, Spectral properties of EEG fast activity ictal discharges associated with infantile spasms. *Clin Neurophysiol* **110**, 593-603 (1999).
2. J. Engel, Jr., A practical guide for routine EEG studies in epilepsy. *J Clin Neurophysiol* **1**, 109-142 (1984).
3. S. Noachtar, J. Remi, The role of EEG in epilepsy: a critical review. *Epilepsy & behavior : E&B* **15**, 22-33 (2009).
4. C. A. Schevon, S. Tobochnik, T. Eissa, E. Merricks, B. Gill, R. R. Parrish, L. M. Bateman, G. M. McKhann, R. G. Emerson, A. J. Trevelyan, Multiscale recordings reveal the dynamic spatial structure of human seizures. *Neurobiol Dis* **127**, 303-311 (2019).
5. J. X. Tao, M. Baldwin, S. Hawes-Ebersole, J. S. Ebersole, Cortical substrates of scalp EEG epileptiform discharges. *J Clin Neurophysiol* **24**, 96-100 (2007).
6. E. R. Kandel, W. A. Spencer, Electrophysiology of hippocampal neurons. II. After-potentials and repetitive firing. *J Neurophysiol* **24**, 243-259 (1961).
7. H. Matsumoto, C. A. Marsan, CORTICAL CELLULAR PHENOMENA IN EXPERIMENTAL EPILEPSY: ICTAL MANIFESTATIONS. *Exp Neurol* **9**, 305-326 (1964).
8. G. Buzsáki, C. A. Anastassiou, C. Koch, The origin of extracellular fields and currents--EEG, ECoG, LFP and spikes. *Nat Rev Neurosci* **13**, 407-420 (2012).
9. C. A. Schevon, S. A. Weiss, G. McKhann, R. R. Goodman, R. Yuste, R. G. Emerson, A. J. Trevelyan, Evidence of an inhibitory restraint of seizure activity in humans. *Nat Commun* **3**, 1060 (2012).
10. M. R. Delucchi, B. Garoutte, R. B. Aird, The scalp as an electroencephalographic averager. *Electroencephalogr Clin Neurophysiol* **14**, 191-196 (1962).
11. E. M. Merricks, E. H. Smith, R. G. Emerson, L. M. Bateman, G. M. McKhann, R. R. Goodman, S. A. Sheth, B. Greger, P. A. House, A. J. Trevelyan, C. A. Schevon, Neuronal Firing and Waveform Alterations through Ictal Recruitment in Humans. *J Neurosci* **41**, 766-779 (2021).
12. J. J. Jun, N. A. Steinmetz, J. H. Siegle, D. J. Denman, M. Bauza, B. Barbarits, A. K. Lee, C. A. Anastassiou, A. Andrei, C. Aydin, M. Barbic, T. J. Blanche, V. Bonin, J. Couto, B. Dutta, S. L. Gratiy, D. A. Gutnisky, M. Hausser, B. Karsh, P. Ledochowitsch, C. M. Lopez, C. Mitelut, S. Musa, M. Okun, M. Pachitariu, J. Putzeys, P. D. Rich, C. Rossant, W. L. Sun, K. Svoboda, M. Carandini, K. D. Harris, C. Koch, J. O'Keefe, T. D. Harris, Fully integrated silicon probes for high-density recording of neural activity. *Nature* **551**, 232-236 (2017).
13. F. Ali, A. C. Kwan, Interpreting in vivo calcium signals from neuronal cell bodies, axons, and dendrites: a review. *Neurophotonics* **7**, 011402 (2020).
14. H. J. Koester, B. Sakmann, Calcium dynamics in single spines during coincident pre- and postsynaptic activity depend on relative timing of back-propagating action potentials and subthreshold excitatory postsynaptic potentials. *Proc Natl Acad Sci U S A* **95**, 9596-9601 (1998).
15. J. H. Bollmann, F. Helmchen, J. G. Borst, B. Sakmann, Postsynaptic Ca2+ influx mediated by three different pathways during synaptic transmission at a calyx-type synapse. *J Neurosci* **18**, 10409-10419 (1998).
16. Y. Schiller, Inter-ictal- and ictal-like epileptic discharges in the dendritic tree of neocortical pyramidal neurons. *J Neurophysiol* **88**, 2954-2962 (2002).
17. T. W. Chen, T. J. Wardill, Y. Sun, S. R. Pulver, S. L. Renninger, A. Baohan, E. R. Schreiter, R. A. Kerr, M. B. Orger, V. Jayaraman, L. L. Looger, K. Svoboda, D. S. Kim, Ultrasensitive fluorescent proteins for imaging neuronal activity. *Nature* **499**, 295-300 (2013).
18. D. Aharoni, B. S. Khakh, A. J. Silva, P. Golshani, All the light that we can see: a new era in miniaturized microscopy. *Nature methods* **16**, 11-13 (2019).
19. K. E. Reyes-Marin, A. Nunez, Seizure susceptibility in the APP/PS1 mouse model of Alzheimer's disease and relationship with amyloid beta plaques. *Brain Res* **1677**, 93-100 (2017).
20. S. F. Muldoon, V. Villette, T. Tressard, A. Malvache, S. Reichinnek, F. Bartolomei, R. Cossart, GABAergic inhibition shapes interictal dynamics in awake epileptic mice. *Brain* **138**, 2875-2890 (2015).

21. L. A. Lau, K. J. Staley, K. P. Lillis, In vitro ictogenesis is stochastic at the single neuron level. *Brain*, (2021).
22. Y. Berdichevsky, V. Dzhala, M. Mail, K. J. Staley, Interictal spikes, seizures and ictal cell death are not necessary for post-traumatic epileptogenesis in vitro. *Neurobiol Dis* **45**, 774-785 (2012).
23. L. Huang, P. Ledochowitsch, U. Knoblich, J. Lecoq, G. J. Murphy, R. C. Reid, S. E. de Vries, C. Koch, H. Zeng, M. A. Buice, J. Waters, L. Li, Relationship between simultaneously recorded spiking activity and fluorescence signal in GCaMP6 transgenic mice. *Elife* **10**, (2021).
24. J. L. Jankowsky, D. J. Fadale, J. Anderson, G. M. Xu, V. Gonzales, N. A. Jenkins, N. G. Copeland, M. K. Lee, L. H. Younkin, S. L. Wagner, S. G. Younkin, D. R. Borchelt, Mutant presenilins specifically elevate the levels of the 42 residue beta-amyloid peptide in vivo: evidence for augmentation of a 42-specific gamma secretase. *Hum Mol Genet* **13**, 159-170 (2004).
25. H. Zhou, K. R. Neville, N. Goldstein, S. Kabu, N. Kausar, R. Ye, T. T. Nguyen, N. Gelwan, B. T. Hyman, S. N. Gomperts, Cholinergic modulation of hippocampal calcium activity across the sleep-wake cycle. *Elife* **8**, (2019).
26. H. Zhou, H. Li, N. Gowravaram, M. Quan, N. Kausar, S. N. Gomperts, Disruption of hippocampal neuronal circuit function depends upon behavioral state in the APP/PS1 mouse model of Alzheimer's disease. *Sci Rep* **12**, 21022 (2022).
27. H. Dana, Y. Sun, B. Mohar, B. K. Hulse, A. M. Kerlin, J. P. Hasseman, G. Tsegaye, A. Tsang, A. Wong, R. Patel, J. J. Macklin, Y. Chen, A. Konnerth, V. Jayaraman, L. L. Looger, E. R. Schreiter, K. Svoboda, D. S. Kim, High-performance calcium sensors for imaging activity in neuronal populations and microcompartments. *Nature methods* **16**, 649-657 (2019).
28. H. Zhou, K. R. Neville, N. Goldstein, S. Kabu, N. Kausar, R. Ye, T. T. Nguyen, N. Gelwan, B. T. Hyman, S. N. Gomperts. (Dryad, 2019).
29. F. Trombin, V. Gnatkovsky, M. de Curtis, Changes in action potential features during focal seizure discharges in the entorhinal cortex of the in vitro isolated guinea pig brain. *J Neurophysiol* **106**, 1411-1423 (2011).
30. E. M. Merricks, E. H. Smith, G. M. McKhann, R. R. Goodman, L. M. Bateman, R. G. Emerson, C. A. Schevon, A. J. Trevelyan, Single unit action potentials in humans and the effect of seizure activity. *Brain* **138**, 2891-2906 (2015).
31. A. Pisani, P. Bonsi, G. Martella, C. De Persis, C. Costa, F. Pisani, G. Bernardi, P. Calabresi, Intracellular calcium increase in epileptiform activity: modulation by levetiracetam and lamotrigine. *Epilepsia* **45**, 719-728 (2004).
32. E. R. Kandel, W. A. Spencer, Excitation and inhibition of single pyramidal cells during hippocampal seizure. *Exp Neurol* **4**, 162-179 (1961).
33. P. A. Rutecki, Y. Yang, Ictal epileptiform activity in the CA3 region of hippocampal slices produced by pilocarpine. *J Neurophysiol* **79**, 3019-3029 (1998).
34. G. L. Westbrook, E. W. Lothman, Cellular and synaptic basis of kainic acid-induced hippocampal epileptiform activity. *Brain Res* **273**, 97-109 (1983).
35. R. R. Parrish, N. K. Codadu, C. Mackenzie-Gray Scott, A. J. Trevelyan, Feedforward inhibition ahead of ictal wavefronts is provided by both parvalbumin- and somatostatin-expressing interneurons. *The Journal of physiology* **597**, 2297-2314 (2019).
36. D. A. Prince, B. J. Wilder, Control mechanisms in cortical epileptogenic foci. "Surround" inhibition. *Arch Neurol* **16**, 194-202 (1967).
37. A. J. Trevelyan, C. A. Schevon, How inhibition influences seizure propagation. *Neuropharmacology* **69**, 45-54 (2013).
38. K. P. Lillis, M. A. Kramer, J. Mertz, K. J. Staley, J. A. White, Pyramidal cells accumulate chloride at seizure onset. *Neurobiol Dis* **47**, 358-366 (2012).
39. T. Jacob, K. P. Lillis, Z. Wang, W. Swiercz, N. Rahmati, K. J. Staley, A Proposed Mechanism for Spontaneous Transitions between Interictal and Ictal Activity. *J Neurosci* **39**, 557-575 (2019).
40. J. DeFelipe, I. Farinas, The pyramidal neuron of the cerebral cortex: morphological and chemical characteristics of the synaptic inputs. *Progress in neurobiology* **39**, 563-607 (1992).
41. J. M. Mungai, Dendritic patterns in the somatic sensory cortex of the cat. *J Anat* **101**, 403-418 (1967).
42. P. L. Nunez, R. Srinivasan, *Electric fields of the brain: the neurophysics of EEG*. (Oxford University Press, USA, 2006).
43. S. Lee, S. S. Deshpande, E. M. Merricks, E. Schlafly, R. Goodman, G. M. McKhann, E. N. Eskandar, J. R. Madsen, S. S. Cash, M. van Putten, C. A. Schevon, W. van Drongelen, Spatiotemporal spike-centered

averaging reveals symmetry of temporal and spatial components of the spike-LFP relationship during human focal seizures. *Commun Biol* **6**, 317 (2023).
44. M. Bazelot, C. Dinocourt, I. Cohen, R. Miles, Unitary inhibitory field potentials in the CA3 region of rat hippocampus. *The Journal of physiology* **588**, 2077-2090 (2010).
45. B. Telenczuk, N. Dehghani, M. Le Van Quyen, S. S. Cash, E. Halgren, N. G. Hatsopoulos, A. Destexhe, Local field potentials primarily reflect inhibitory neuron activity in human and monkey cortex. *Sci Rep* **7**, 40211 (2017).
46. M. Telenczuk, B. Telenczuk, A. Destexhe, Modelling unitary fields and the single-neuron contribution to local field potentials in the hippocampus. *The Journal of physiology* **598**, 3957-3972 (2020).
47. A. J. Trevelyan, S. F. Muldoon, E. M. Merricks, C. Racca, K. J. Staley, The role of inhibition in epileptic networks. *J Clin Neurophysiol* **32**, 227-234 (2015).
48. P. Jiruska, M. de Curtis, J. G. Jefferys, C. A. Schevon, S. J. Schiff, K. Schindler, Synchronization and desynchronization in epilepsy: controversies and hypotheses. *The Journal of physiology* **591**, 787-797 (2013).
49. M. Levesque, D. Ragsdale, M. Avoli, Evolving Mechanistic Concepts of Epileptiform Synchronization and their Relevance in Curing Focal Epileptic Disorders. *Curr Neuropharmacol* **17**, 830-842 (2019).
50. L. Rubi, U. Schandl, M. Lagler, P. Geier, D. Spies, K. D. Gupta, S. Boehm, H. Kubista, Raised activity of L-type calcium channels renders neurons prone to form paroxysmal depolarization shifts. *Neuromolecular Med* **15**, 476-492 (2013).
51. V. Stiglbauer, M. Hotka, M. Ruiss, K. Hilber, S. Boehm, H. Kubista, Cav 1.3 channels play a crucial role in the formation of paroxysmal depolarization shifts in cultured hippocampal neurons. *Epilepsia* **58**, 858-871 (2017).
52. K. L. Powell, S. M. Cain, T. P. Snutch, T. J. O'Brien, Low threshold T-type calcium channels as targets for novel epilepsy treatments. *Br J Clin Pharmacol* **77**, 729-739 (2014).
53. M. Wenzel, J. P. Hamm, D. S. Peterka, R. Yuste, Acute Focal Seizures Start As Local Synchronizations of Neuronal Ensembles. *J Neurosci* **39**, 8562-8575 (2019).
54. X. Zhang, Z. Qiao, N. Liu, L. Gao, L. Wei, A. Liu, Z. Ma, F. Wang, S. Hou, J. Li, H. Shen, Stereotypical patterns of epileptiform calcium signal in hippocampal CA1, CA3, dentate gyrus and entorhinal cortex in freely moving mice. *Sci Rep* **9**, 4518 (2019).
55. T. K. Berdyyeva, E. P. Frady, J. J. Nassi, L. Aluisio, Y. Cherkas, S. Otte, R. M. Wyatt, C. Dugovic, K. K. Ghosh, M. J. Schnitzer, T. Lovenberg, P. Bonaventure, Direct Imaging of Hippocampal Epileptiform Calcium Motifs Following Kainic Acid Administration in Freely Behaving Mice. *Frontiers in neuroscience* **10**, 53 (2016).
56. M. Wenzel, J. P. Hamm, D. S. Peterka, R. Yuste, Reliable and Elastic Propagation of Cortical Seizures In Vivo. *Cell Rep* **19**, 2681-2693 (2017).
57. L. Stoppini, P. A. Buchs, D. Muller, A simple method for organotypic cultures of nervous tissue. *J Neurosci Methods* **37**, 173-182 (1991).
58. V. I. Dzhala, K. J. Staley, KCC2 Chloride Transport Contributes to the Termination of Ictal Epileptiform Activity. *eNeuro* **8**, (2021).
59. T. A. Pologruto, B. L. Sabatini, K. Svoboda, ScanImage: flexible software for operating laser scanning microscopes. *Biomed Eng Online* **2**, 13 (2003).
60. J. Schindelin, I. Arganda-Carreras, E. Frise, V. Kaynig, M. Longair, T. Pietzsch, S. Preibisch, C. Rueden, S. Saalfeld, B. Schmid, J. Y. Tinevez, D. J. White, V. Hartenstein, K. Eliceiri, P. Tomancak, A. Cardona, Fiji: an open-source platform for biological-image analysis. *Nat Methods* **9**, 676-682 (2012).

Funding:

National Institutes of Health grant R01NS112538 (KPL)
National Institutes of Health grant R35NS116852 (KJS)
National Institutes of Health grant R01AG054551 (SNG)

Author contributions:

Conceptualization: LAL, KPL, KJS

Methodology: LAL, KLP, KJS
Investigation: LAL, ZZ
Formal analysis: LAL
Funding acquisition: KPL, KJS, SNG
Writing – original draft: LAL, KPL, KJS
Writing – review & editing: LAL, ZZ, SNG, KPL, KJS

Competing interests: Authors declare that they have no competing interests.

Data and materials availability: Data generated from this study is available upon reasonable request from the corresponding author.

Figures

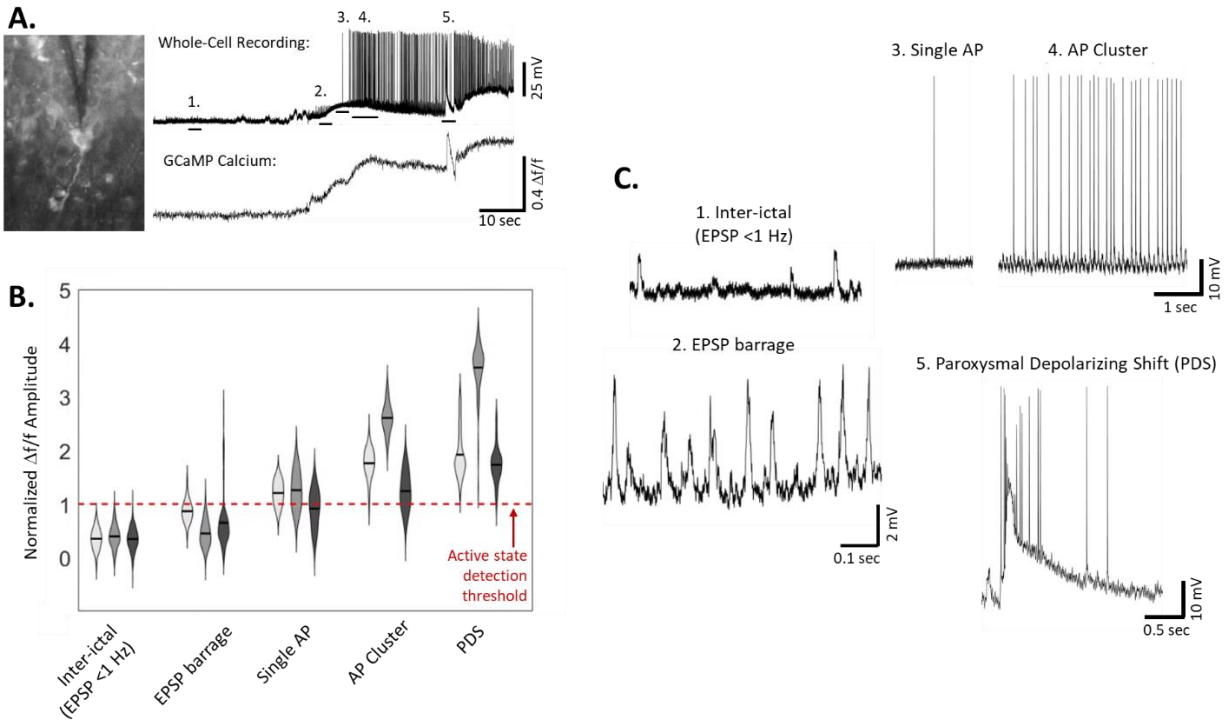

Fig. 1. Paired calcium imaging and whole-cell patch clamp. (**A**) Left: Image of GCaMP+ neuron and patch pipette in OHSC. Right: Paired current-clamp recording and soma-GCaMP8m calcium signal (Δf/f) during spontaneous seizure. (**B**) Violin plot of calcium Δf/f amplitudes during different types of electrical activity, normalized to active state detection threshold per cell. (n = 3 neurons, from 3 OHSCs). (**C**) Zoom-in to each category of electrical activity, as noted in (A). 1- Inter-ictal activity: period between seizures where EPSPs frequency is below 1 Hz. 2- EPSP barrage: typically seen at seizure onset, with EPSP frequency >1 Hz. 3- Single Action Potential (AP): single AP in a 150 ms window. 4- AP Cluster: 10+ action potentials with <150 ms inter-spike interval. 5- Paroxysmal depolarizing shift (PDS): characterized by action potentials on top of a depolarized plateau of 20-50 mV, lasting tens-hundreds of ms.

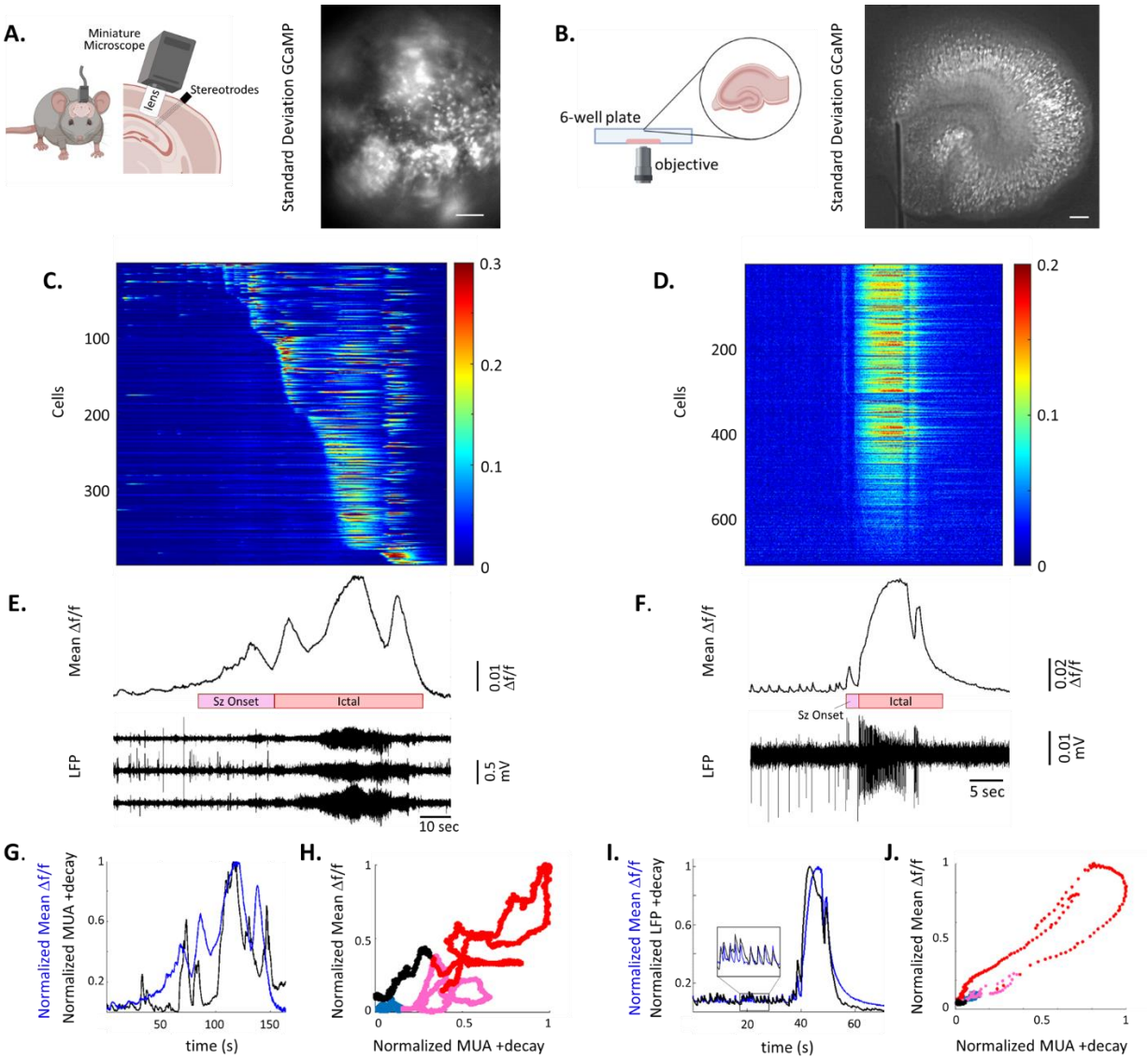

Fig. 2. Paired calcium imaging and local field potential in vivo and in vitro. (**A**) Left: schematic of in vivo imaging. Right: Representative image of standard deviation projection during syn-GCaMP6f calcium imaging. Scale bar = 100 µm. (**B**) Left: Schematic of in vitro imaging. Right: Representative image of standard deviation projection during syn-GCaMP7f calcium imaging. Scale bar = 100 µm. (**C**) Raster plot of GCaMP6f Δf/f of individual neurons during in vivo seizure (**D**) Raster plot of GCaMP7f Δf/f of individual neurons during in vitro seizure (**E**) Paired mean GCaMP6f Δf/f trace and 3 channels of local field potential (LFP), in vivo. (**F**) Paired mean GCaMP7f Δf/f trace and LFP, in vitro. (**G**) Plot of normalized local field potential activity that has been high-pass filtered at 300 Hz for multiunit activity (MUA), rectified and down-sampled to

rate of imaging (black) and normalized mean Δf/f calcium (blue), simultaneously recorded during in vivo seizure (**H**) Correlation in signal between the two modalities, color indicates phase of seizure (blue = baseline inter-ictal; pink = seizure onset; red = ictal; black = post-ictal). (**I**) Plot of normalized local field potential activity that has been rectified and down-sampled to rate of imaging (black) and normalized mean Δf/f calcium (blue), simultaneously recorded during in vitro seizure (**J**) Correlation in signal between the two modalities, color indicates phase of seizure (blue = baseline inter-ictal; pink = seizure onset; red = ictal; black = post-ictal).

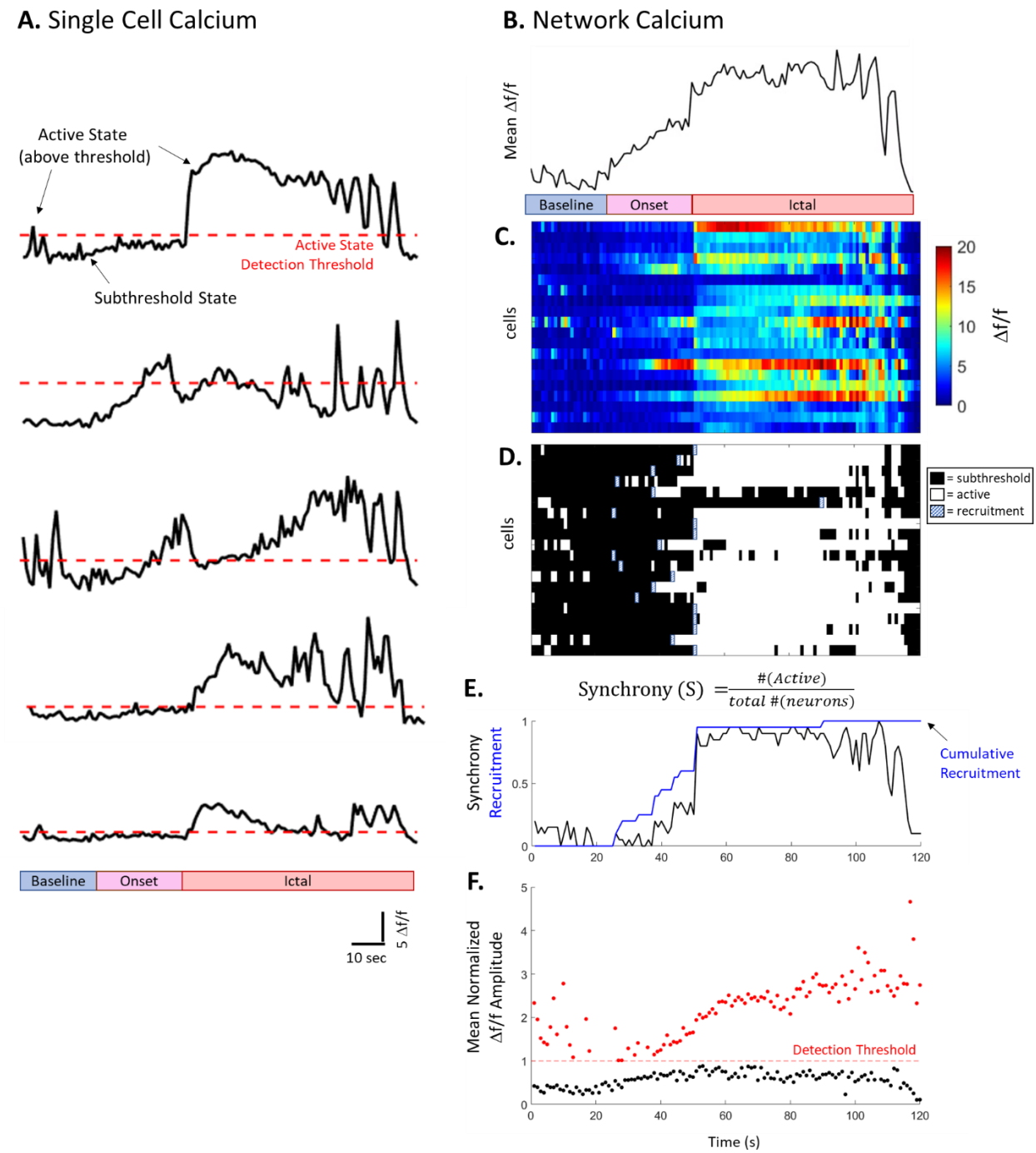

Fig. 3. Changes in network synchrony and calcium amplitude underly population level changes. (**A**) Example single cell calcium traces. Red line indicates active state detection threshold for each cell. Phase of seizure indicated by colorbar. (**B**) Top: Mean Δf/f calcium of 20 neurons. (**C**) Raster plot showing the Δf/f amplitude for each of the 20 neurons. Neurons in (A) correspond to cell #1, 5, 10, 15 and 20 in raster plot. (**D**) Raster

plot depicting when neurons are in the subthreshold (black) or active states (white). Recruitment shown in hatched white/blue and represents the first time a neuron is in the active state during the seizure epoch. (**E**) Plot of network synchrony over time (i.e. fraction of network in the active state). Blue line = cumulative recruitment. (**F**) Scatter plot of the mean active (red) and subthreshold (black) Ca^{+2} $\Delta f/f$ amplitude over time normalized to detection threshold (red dotted line). Number of cells contributing to mean varies over time depending on number of neurons in active versus subthreshold state at each time point.

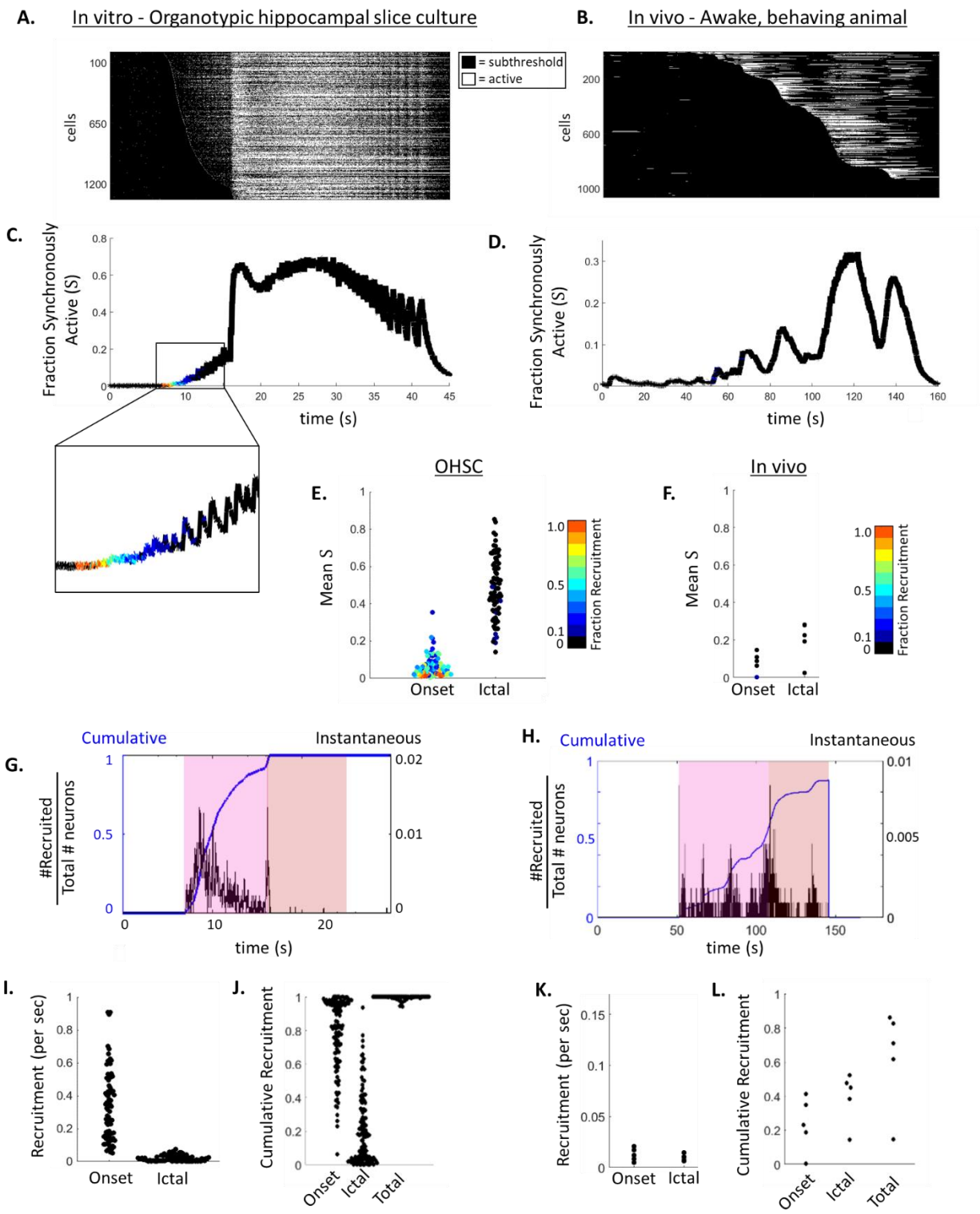
A.
In vitro - Organotypic hippocampal slice culture
= subthreshold
= active
cells
B.
In vivo - Awake, behaving animal
C.
Fraction Synchronously Active (S)
time (s)
D.
OHSC
In vivo
E.
F.
Mean S
Onset
Ictal
Fraction Recruitment
G.
H.
Cumulative
Instantaneous
#Recruited / Total # neurons
I.
J.
K.
L.
Recruitment (per sec)
Cumulative Recruitment
Total

Fig. 4. Network synchrony and recruitment. (**A**) Raster plot of depicting when neurons are in subthreshold (black) or active state (white) during seizure recorded from OHSC. Cells are sorted by recruitment order. (**B**) Raster plot of depicting when neurons are in subthreshold (black) or active state (white) during seizure recorded in vivo. Cells are sorted by recruitment order. (**C**) Plot of fraction of synchronously active neurons (S = # active neurons/total # neurons) over time from seizure in (A). Color represents fraction of S that is new recruitment. (**D**) Plot of fraction of synchronously active neurons (S = # active neurons/total # neurons) over time from seizure in (B). Color represents fraction of S that is new recruitment. (**E**) Beeswarm plot of time-averaged fraction of synchronously active neurons (S) during seizure onset and ictal activity. Colorbar = recruitment/total fraction active. n = 82 seizures from OHSCs. (**F**) Beeswarm plot of time-averaged fraction of synchronously active neurons (S) during seizure onset and ictal. Colorbar = mean recruitment/total fraction active. n = 5 in vivo seizures. (**G**) Plot of instantaneous recruitment (black) and cumulative recruitment (blue), from same seizure in (A) and (C). (**H**) Plot of instantaneous recruitment (black) and cumulative recruitment (blue), from same seizure in (B) and (D). (**I**) Beeswarm plot of mean rate of recruitment (fraction of total network recruited per second) during onset and ictal periods, n = 82 seizures from OHSCs. (**J**) Beeswarm plot of cumulative recruitment during onset, ictal and in total (onset + ictal), n = 82 seizures from OHSCs. (**K**) Beeswarm plot of mean rate of recruitment (fraction of total network recruited per second) during onset and ictal periods, n = 5 in vivo seizures. (**L**) Beeswarm plot of cumulative recruitment during onset, ictal and in total, n = 5 in vivo seizures.

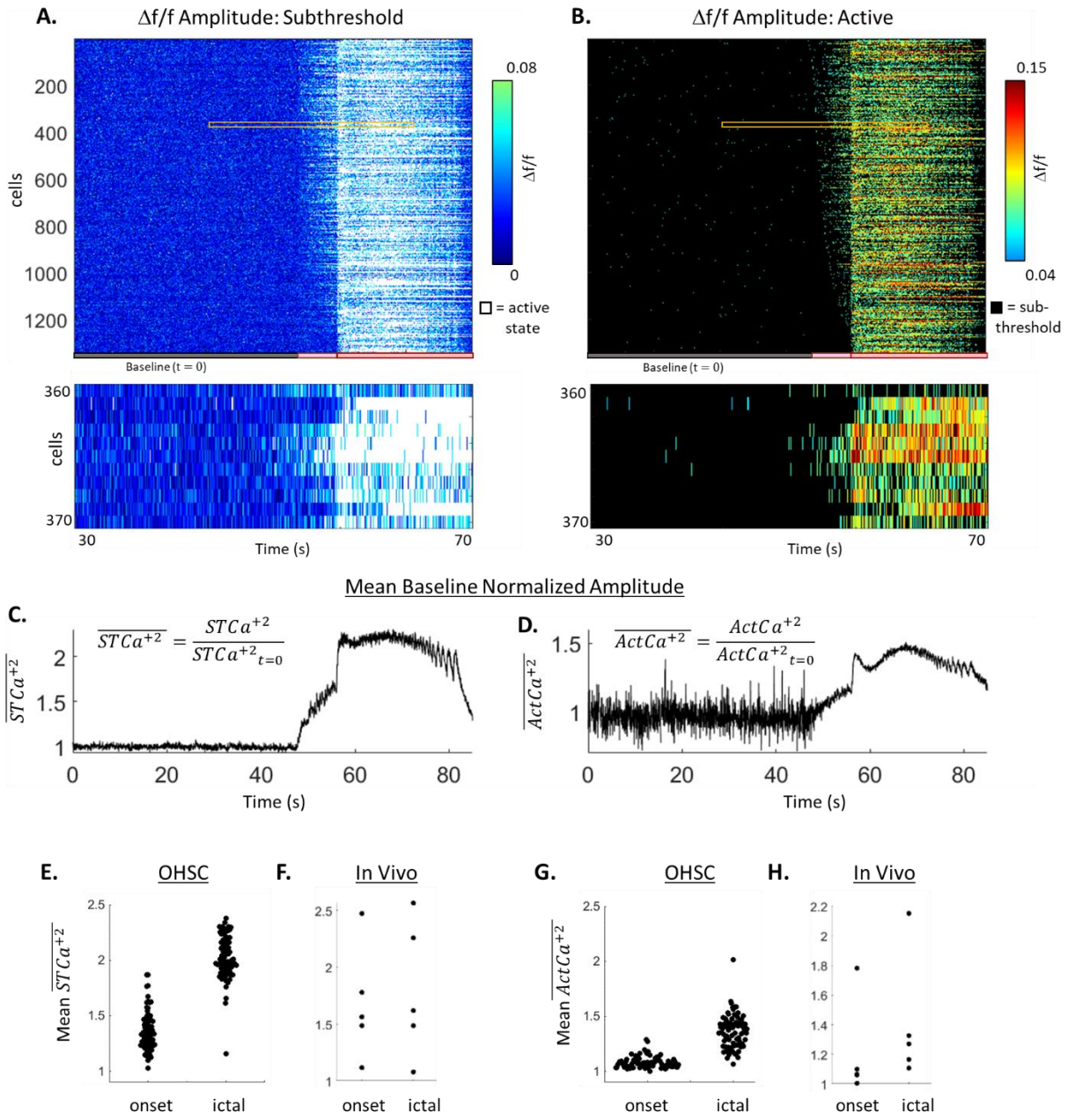

Fig. 5. Change in calcium amplitude (**A**) Raster plot of Δf/f signal of neurons in the subthreshold state. White = time points when the neuron was in the active state. Colors on bottom show stages of activity, gray = baseline activity, pink = seizure onset, red = ictal. Bottom: zoom-in to 40 seconds of activity in 10 cells. (**B**) Raster plot of Δf/f signal of neurons in the active state. Black = time points when the neuron was subthreshold. Bottom: zoom-in to 40 seconds of activity in 10 cells. (**C**) Example mean baseline normalized subthreshold calcium ($STCa^{+2}$) amplitude over time of all neurons shown in

(A). (**D**) Example mean baseline normalized active calcium ($ActCa^{+2}$) amplitude over time of all neurons shown in (B). Data from A-D all show the same seizure recorded from a OHSC. (**E**) Beeswarm plot of time-averaged mean normalized $STCa^{+2}$ amplitude during seizure onset and ictal in OHSC. n = 82 seizures. (**F**) Beeswarm plot of time-averaged mean normalized $STCa^{+2}$ amplitude during seizure onset and ictal in vivo. n = 5 seizures. (**G**) Beeswarm plot of time-averaged mean normalized $ActCa^{+2}$ amplitude during seizure onset and ictal in OHSC. (**H**) Beeswarm plot of time-averaged mean normalized $ActCa^{+2}$ amplitude during seizure onset and ictal activity in vivo.

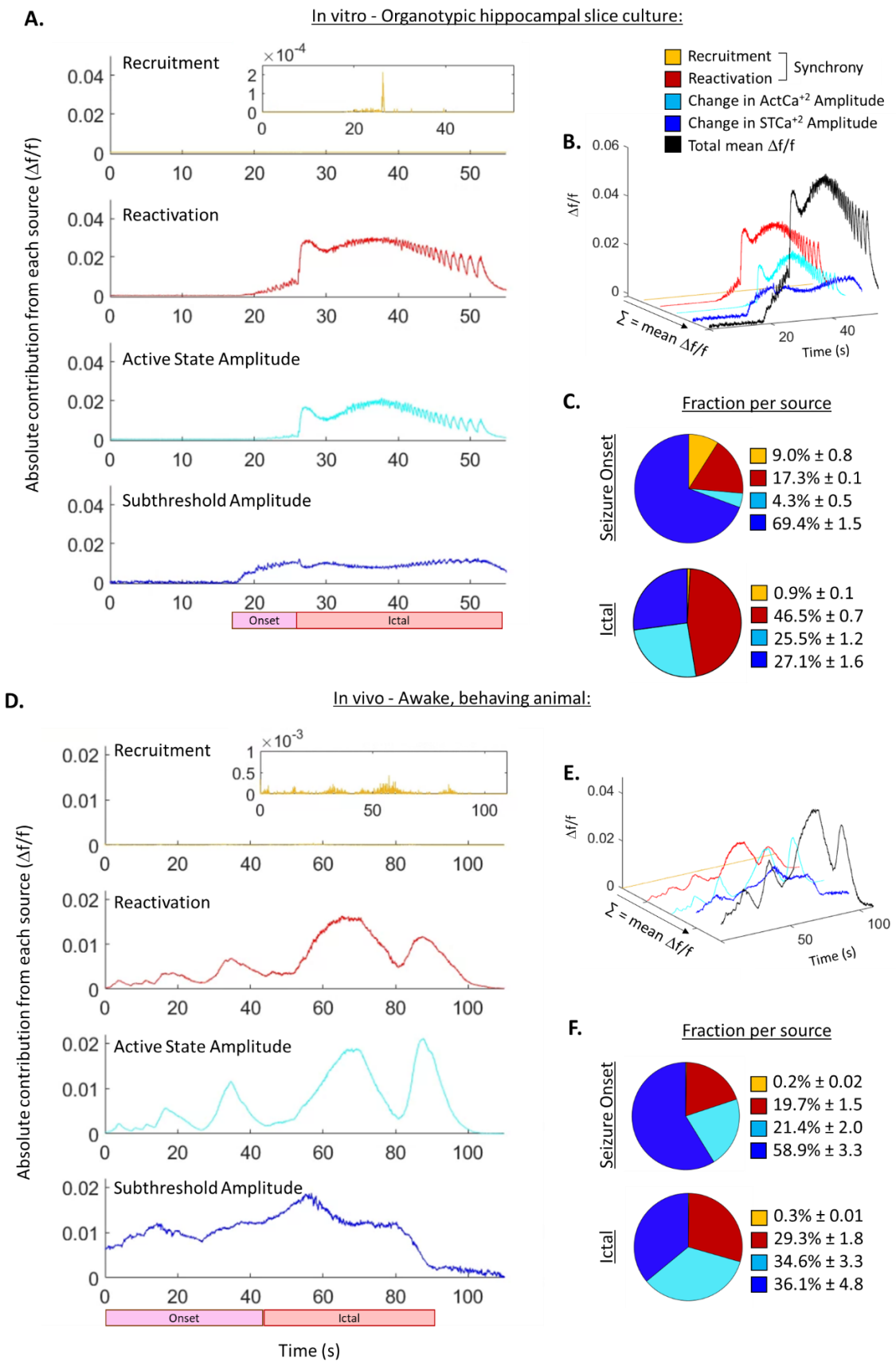
A.
In vitro - Organotypic hippocampal slice culture:
Recruitment
Reactivation
Active State Amplitude
Subthreshold Amplitude
Absolute contribution from each source (Δf/f)
Onset
Ictal
B.
Recruitment
Reactivation
Synchrony
Change in ActCa+2 Amplitude
Change in STCa+2 Amplitude
Total mean Δf/f
Δf/f
Σ = mean Δf/f
Time (s)
C.
Fraction per source
Seizure Onset
9.0% ± 0.8
17.3% ± 0.1
4.3% ± 0.5
69.4% ± 1.5
Ictal
0.9% ± 0.1
46.5% ± 0.7
25.5% ± 1.2
27.1% ± 1.6
D.
In vivo - Awake, behaving animal:
Recruitment
Reactivation
Active State Amplitude
Subthreshold Amplitude
Absolute contribution from each source (Δf/f)
Onset
Ictal
Time (s)
E.
Δf/f
Σ = mean Δf/f
Time (s)
F.
Fraction per source
Seizure Onset
0.2% ± 0.02
19.7% ± 1.5
21.4% ± 2.0
58.9% ± 3.3
Ictal
0.3% ± 0.01
29.3% ± 1.8
34.6% ± 3.3
36.1% ± 4.8

Fig. 6. Quantifying sources of increased population calcium signal during seizure (**A**) Plots of the absolute contributions of recruitment, reactivation, change in mean active calcium amplitude ($ActCa^{+2}$), and mean subthreshold calcium amplitude ($STCa^{+2}$) in an example seizure recorded from an OHSC. (**B**) 3D line plot of the 4 sources of ictal signal and the total mean Δf/f signal in black from the example seizure in (A). The 4 sources (recruitment (yellow), reactivation (red), changing in $ActCa^{+2}$ (cyan), and change in $STCa^{+2}$ amplitude(blue)) summate into the population level mean Δf/f signal (black). (**C**) Pie chart of the mean relative contribution of each source during seizure onset and ictal activity, n = 82 seizures from OHSC. Relative contribution = absolute contribution/total Δf/f signal. (**D**) Plots of the absolute contributions of recruitment, reactivation, change in mean active calcium amplitude ($ActCa^{+2}$), and mean subthreshold calcium amplitude ($STCa^{+2}$) in an example seizure recorded in vivo. (**E**) 3D line plot of the 4 sources of ictal signal and the total mean Δf/f signal in black from the example seizure in (D). The 4 sources (recruitment (yellow), reactivation (red), changing in $ActCa^{+2}$ (cyan), and change in $STCa^{+2}$ amplitude(blue)) summate into the population level mean Δf/f signal (black). (**F**) Pie chart of the mean relative contribution of each source during seizure onset and ictal activity, n = 5 in vivo seizures. Relative contribution = absolute contribution/total Δf/f signal.

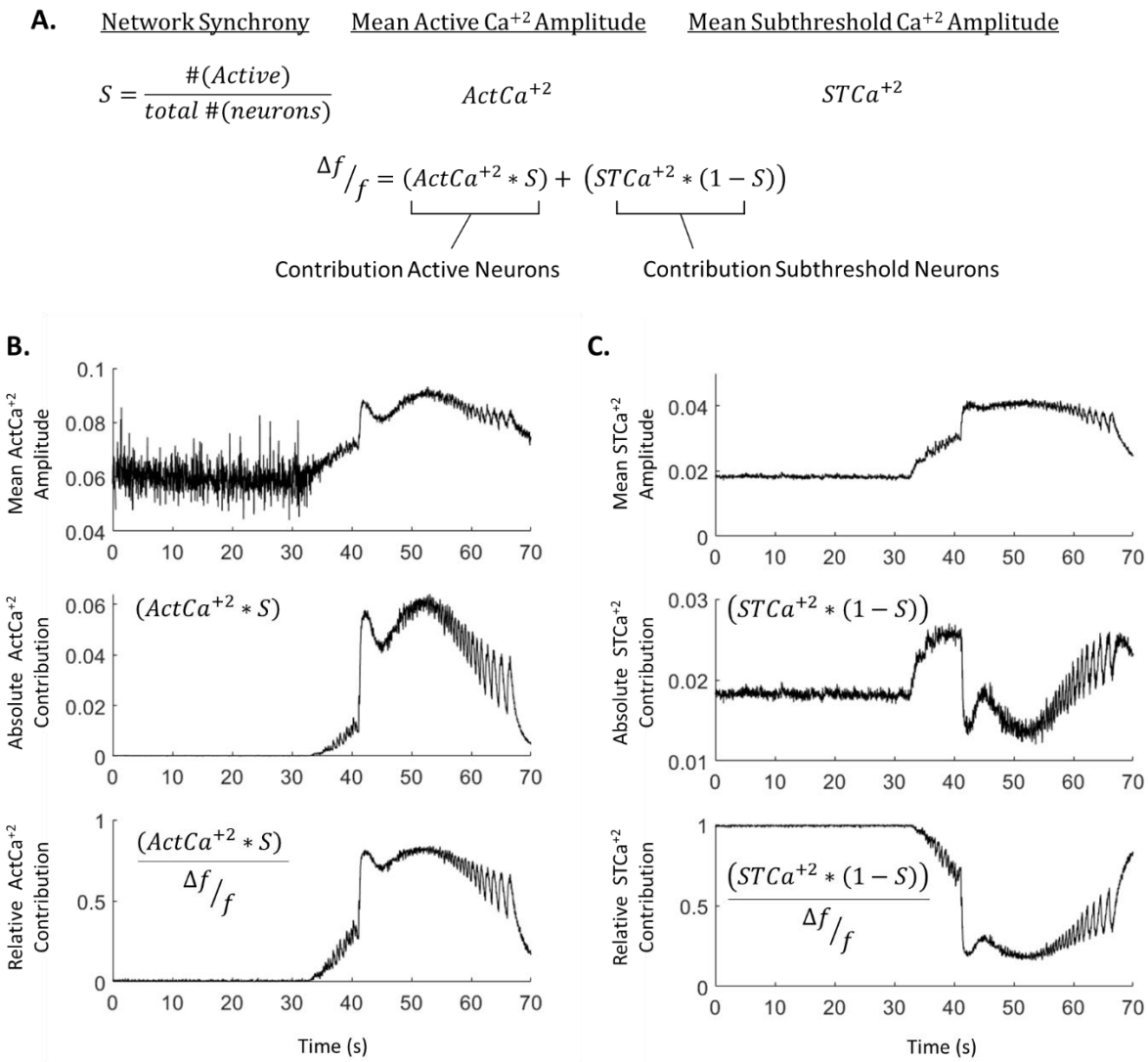

Fig. 7. Quantifying contribution from active and subthreshold neurons (**A**) Equation for quantifying the contribution from active neurons and subthreshold neurons, which can be calculated from 3 terms: network synchrony ($S = \frac{\#(ActCa^{+2})}{total\ \#(neurons)}$), mean active calcium amplitude ($ActCa^{+2}$), and mean subthreshold calcium amplitude ($STCa^{+2}$). (**B**) Example plot of the mean $ActCa^{+2}$ amplitude over time, absolute contribution of active state neurons over time ($ActCa^{+2}$ amplitude * fraction of active neurons), and relative contribution of active state neurons (($ActCa^{+2}$ amplitude * fraction of active neurons)/total Δf/f signal) over time from an example seizure in OHSC. (**C**) Example plot of the mean $STCa^{+2}$ amplitude over time, absolute contribution of subthreshold neurons over time ($STCa^{+2}$ amplitude * fraction of subthreshold neurons), and relative contribution of subthreshold neurons (($STCa^{+2}$ amplitude * fraction of subthreshold neurons)/total Δf/f signal) over time from an example seizure in OHSC.

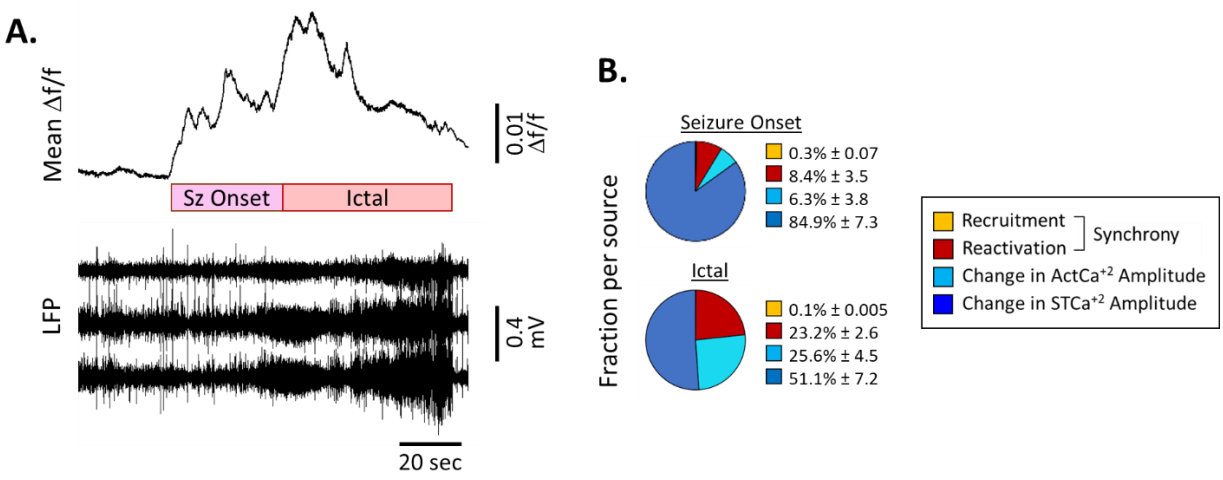

Supplemental Fig. 1. Quantifying sources of increased population calcium signal during type II seizure (**A**) Example mean Δf/f calcium trace and paired local field potential (LFP) during a type II seizure recorded in vivo. Type II defined by high amplitude calcium activity which precedes increased electrical activity by several seconds. (**B**) Pie chart = mean percent of population increase from each source for type II seizures (recruitment, synchrony, change in active Ca^{+2} amplitude, change in subthreshold Ca^{+2} amplitude), n = 3 seizures.

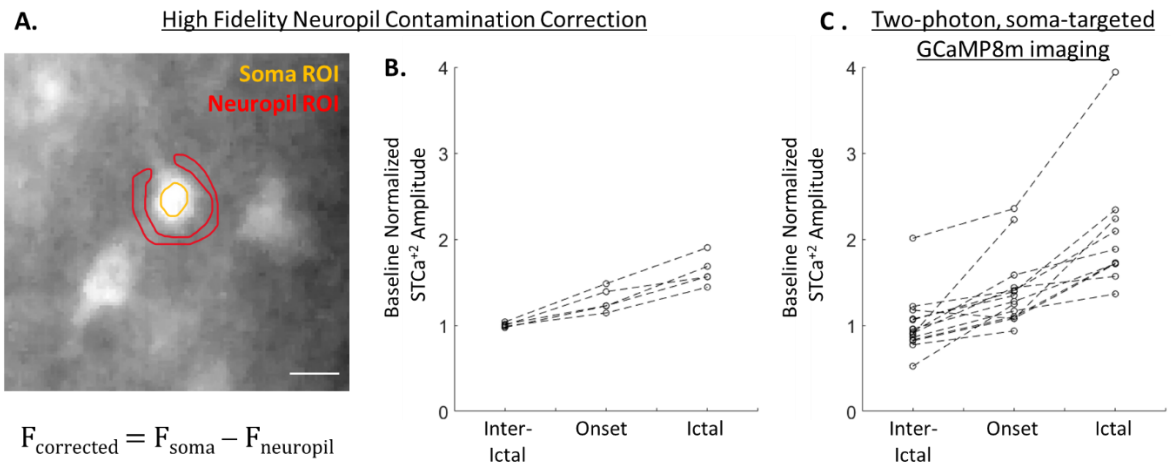

Supplemental Fig. 2. Subthreshold amplitude changes robust to neuropil contamination corrections (**A**) Example of hand drawn soma and neuropil regions of interest in one-photon, GCaMP7f imaging. Scale bar = 10 µm. (**B**) Subthreshold calcium amplitude (normalized to baseline) during inter-ictal, onset and ictal periods with high fidelity neuropil contamination correction. n = 5 neurons; $p = 0.003$ (inter-ictal versus onset) and $p < 0.001$ (inter-ictal versus ictal), paired t-test. (**C**) Subthreshold calcium amplitude (normalized to baseline) during inter-ictal, onset and ictal periods in two-photon, soma-targeted GCaMP8m imaging. n = 15 neurons; $p < 0.001$ (inter-ictal versus onset) and $p < 0.001$ (inter-ictal versus ictal), paired t-test.

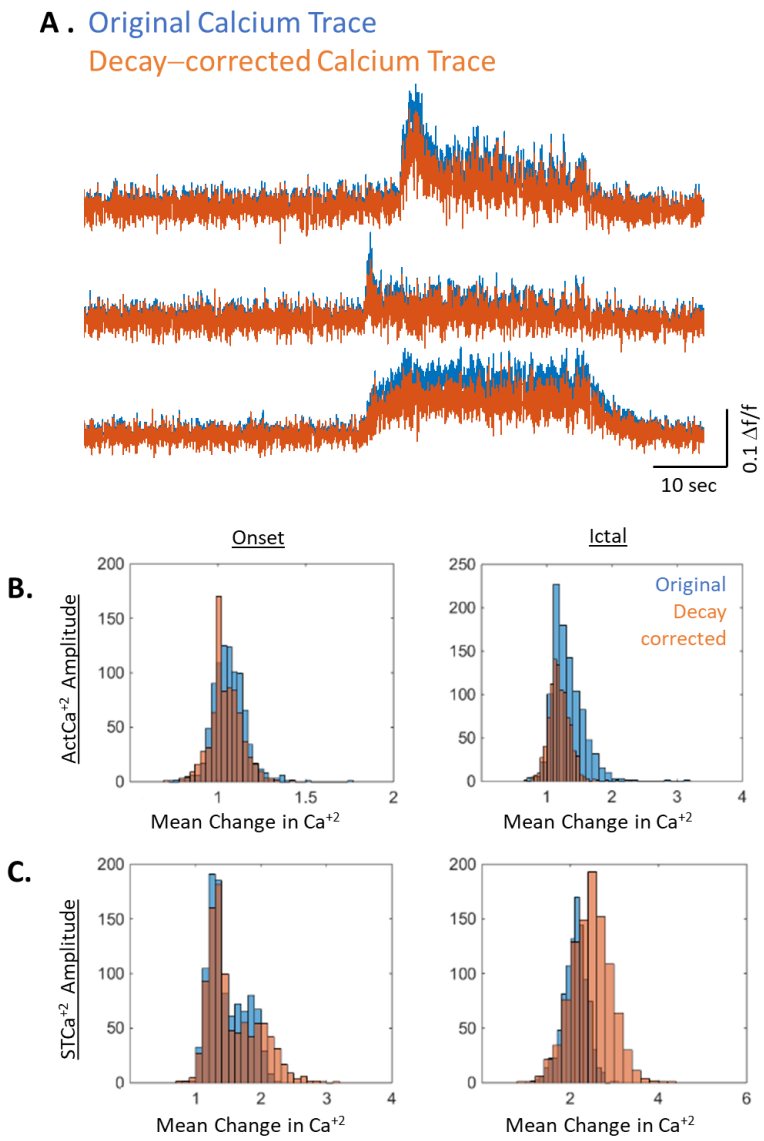

Supplemental Fig. 3. Active state calcium amplitude increases robust to GCaMP decay kinetic correction (**A**) Example calcium traces from individual neurons (original: blue) and after subtraction of GCaMP7f decay kinetics (blue). (**B**) Histograms of the mean change in the active state calcium amplitude during seizure onset and ictal period from original (blue) and decay subtracted (orange) data (**C**) Histograms of the mean change in the subthreshold calcium amplitude during seizure onset and ictal period from original (blue) and decay subtracted (orange) data.

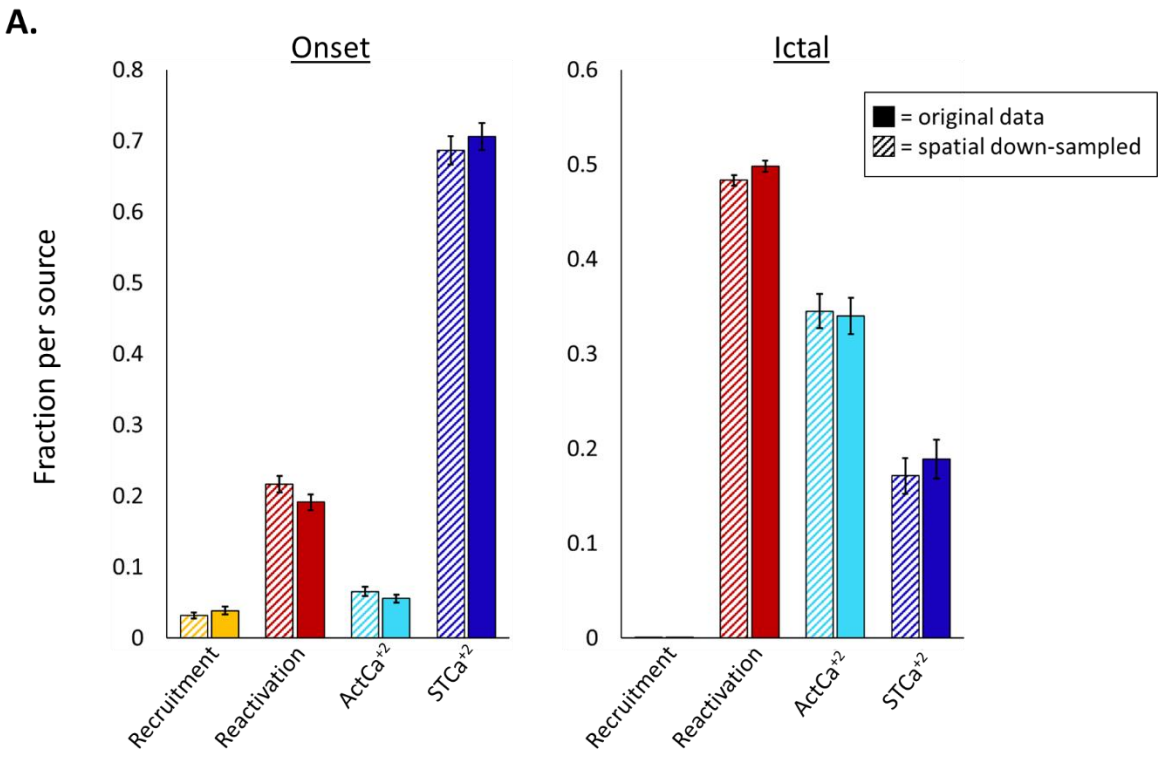

Supplemental Fig. 4. Quantifying sources of increased population calcium signal after spatial subsampling (**A**) Mean percent of population increase from each source during seizure onset (recruitment, synchrony, change in active Ca^{+2} amplitude, change in subthreshold Ca^{+2} amplitude), n = 20 seizures in OHSC. Subsampling was performed by averaging the signal of neurons that fell within 14 μm of each other. (**B**) Mean percent of population increase from each source during ictal activity.